

NASA Contractor Report 3951

Damage Tolerant Composite Wing Panels for Transport Aircraft

Peter J. Smith and Robert D. Wilson

CONTRACT NAS1-16863
DECEMBER 1985

(NASA-CR-3951) DAMAGE TOLERANT COMPOSITE
WING PANELS FOR TRANSPORT AIRCRAFT (Boeing
Commercial Airplane Co.) 60 p CSCL 11D N89-15187
H1/24 Unclas
0184817

release will be three (3) years from date indicated on
the document.

(NASA-CR-3951) DAMAGE TOLERANT COMPOSITE
WING PANELS FOR TRANSPORT AIRCRAFT (Boeing
Commercial Airplane Co.) 60 p LIMIT X86-10344
DOMESTIC Unclas
H1/24 16058

NASA

NASA Contractor Report 3951

Damage Tolerant Composite Wing Panels for Transport Aircraft

Peter J. Smith and Robert D. Wilson
Boeing Commercial Airplane Company
Seattle, Washington

Prepared for
Langley Research Center
under Contract NAS1-16863



National Aeronautics
and Space Administration

Scientific and Technical
Information Branch

1985

DAMAGE TOLERANT COMPOSITE WING PANELS FOR COMMERCIAL TRANSPORT AIRCRAFT

Peter J. Smith and Robert D. Wilson
Advanced Composite Development Program

Boeing Commercial Airplane Company
Seattle, Washington

ABSTRACT

Analysis and testing that addressed the key technology areas of durability and damage tolerance were completed for advanced composite commercial aircraft wing surface panels. The wing of a fuel-efficient, 200-passenger airplane for 1990 delivery was sized using graphite-epoxy materials. The damage tolerance program was structured to allow a systematic progression from material evaluations to the optimized large panel verification tests. The program included coupon testing to evaluate toughened material systems; static and fatigue tests of compression coupons with varying amounts of impact damage, element tests of three-stiffener panels to evaluate upper wing panel design concepts, and a study of the wing structure damage environment. The program was completed with a series of technology demonstration tests of large compression panels. A repair investigation was included in the final large panel test. The results of the program provide key technology data necessary for a 1990s composite wing.

NOMENCLATURE

A	area (in ²)
deg	degree
E	Young's modulus (msi)
G	shear modulus (msi)
Gt/Nx	nondimensional shear stiffness parameter
in	inch
kip	1000 lb
ksi	1000 lb/in ²
lb	pound
lb/in ³	pound per cubic inch
msi	1,000,000 lb/in ²
Nx	end load (kip/in)
P	total panel load (kip)
t	thickness (in)
(xx/yy/zz)	fiber percentage in the laminate (0 deg/45 deg/90 deg)
TTU	thru-transmission ultrasonic inspection
NDE	nondestructive evaluation
R	stress ratio $\left(\frac{P_{\min}}{P_{\max}}\right)$

All dimensions are in inches.

INTRODUCTION

The utilization of advanced composites in the design of a wing box of a commercial transport aircraft requires information from several key technology areas. Under the NASA Large Composite Primary Structure (LCPAS) program Boeing addressed two of these key technology areas, durability and damage tolerance. Because the wing surface panels for a commercial transport aircraft typically represent 65% to 70% of the wing box mass, the emphasis of the LCPAS program was directed at these surface panels.

Weight and cost are generally traded at established dollar per pound of weight reduction ratios for structural design. In the near future, a wing box mass reduction of approximately 20% may be compatible with affordable costs of advanced composite when compared to aluminum designs. To achieve a total wing box mass reduction of 20%, it is necessary to reduce the mass of the wing surface panels by 30% in order to compensate for the presence of metal fittings, joints, and fasteners which cannot be replaced by graphite-epoxy material. To reach the mass reduction goal of 30% in the wing surface panels, a usable design strain of 0.006 in both tension and compression is necessary. This represents a significant increase over the current industry graphite-epoxy design strains of 0.005 for tension and 0.004 for compression. Design strains must contain an adequate reserve to allow for damage tolerance and durability requirements.

The Boeing program was performed in two phases. Phase I was directed to the development of generic technology through tests of toughened composite materials and the evaluation of compression panels. Phase I results are reported in reference 1 and are summarized herein. The present report covers the Phase II effort to develop and demonstrate composite wing panels that meet the goal of a 30% mass reduction and ultimate design strains of 0.006 with simulated service damage.

Use of commercial products or names of manufacturers in this report does not constitute official endorsement of such products or manufacturers, either expressed or implied, by the National Aeronautics and Space Administration.

PHASE I SUMMARY

Phase I of the program was directed toward the development of the generic technology through a series of coupon and three-stiffener compression panel tests. A limited preliminary design study was made of a fuel-efficient high aspect ratio 200-passenger commercial airplane wing. The strength, stiffness, and fatigue requirements were established in this study with the theoretical mass distribution obtained from the aluminum wing design. The airplane configuration and internal loads and stiffness requirements for the wing are documented in Reference 1. The area of the wing selected for study was the upper wing panel at the nacelle, where end loads approach 30 kips/in and the shear stiffness requirement is $G_t=1200$ kips/in ($G_t/Nx=40$).

The graphite-epoxy wing panels were required to work to 48 ksi in order to achieve the 30% mass reduction goal. The extensional modulus selected was 8 msi which allowed the graphite panels to meet the stiffness and damage tolerance requirements. The above stress and stiffness values result in a design strain level of 0.006. Current technology material systems had not demonstrated 0.006 after impact damage; therefore, a material improvement was required to meet the LCPAS objectives. After an evaluation of several toughened materials, the Hercules AS4/2220-3 material was selected.

The fracture, compression strength after impact, and durability characteristics of the Hercules AS4/2220-3 material were evaluated at coupon level testing against the current Narmco T300/5208 as a baseline. The results of the coupon tests indicated improved static strength performance of the AS4/2220-3 material over that of the T300/5208. The results also showed that compression after impact is the critical damage/loading combination for graphite-epoxy. The tests confirmed that graphite-epoxy laminates with typical fastener penetrations have good fatigue performance when designed to ultimate strains of 0.006.

The baseline aluminum design featured a thick skin in order to meet the shear stiffness requirements of the high aspect ratio wing. The skin carries 65% of the end load and the aluminum panels were designed by long-column stability between ribs.

The Phase I graphite-epoxy panel designs typically had softer skins which met the shear stiffness requirements while carrying less end load. These panel configurations were critical for impact damage rather than the Euler column buckling of the aluminum design.

The panel configurations evaluated in Phase I were an I-stiffened design with a relatively stiff skin (30/60/10), a J-stiffened design with a (19/62/19) skin, and embedded 0-deg planks in the skin under the stiffeners, and an integral blade stiffened design with a soft skin (10/80/10). Each design was tested in the three-stiffener panel configuration with various damages representing the ultimate, limit, and continued safe flight criteria established by the FAA and Boeing. These damages varied from skin impacts with a 0.50-in diameter steel impactor to a severed stringer cap. The results of the Phase I panel tests showed that the soft skins (10/80/10) were more damage tolerant than the stiffener 0-deg dominated skins. The panel tests also showed that the overall damage tolerance performance was better for the discrete I- or J-stiffened panels than for the integral blade stiffened panels. These results are documented in Reference 1. The demonstrated ultimate upper surface compression strain capability was 0.005 with barely visible damage. While this capability did not meet the 0.006 program goal, it was a significant increase over previous composite compression panel capability and provided a mass reduction of 24% compared to aluminum panel designs.

PHASE II APPROACH

The principal objective of Phase II was to improve the composite wing panel capability to meet the original goal of 30% mass reduction and allow ultimate design strains of 0.006 in both upper and lower surfaces with impact damage. The Phase II damage tolerance panel development program was structured to allow a systematic progression toward the final large panel verification tests. The results of Phase I indicated that still tougher materials and improved design configurations were needed in order to achieve the program goals. To more fully understand the damage scenario, an in-depth assessment of the wing structure damage environment was to be performed. This required an investigation into the damage threat, manufacturing and quality control processes, service maintenance and inspection practices, and service histories of commercial airplane wings. This investigation was to focus on important aspects of quality control and damage detection and to provide timely conclusions for the design of the final damage tolerant panels.

As part of further design improvement, several toughened material systems were to be evaluated for use in the large panel validation tests. NASA standard test coupon configurations and procedures per Reference 2 were to be used to screen these materials. In addition to these material screening tests, a damage growth test program was included in Phase II in order to evaluate the damage growth characteristics of impact damaged coupons after load cycling. Through-the-thickness stitching was also to be evaluated to measure improvements in impact damage containment and effects on damage growth.

Further damage growth testing was to be performed on three-stiffener panels in order to evaluate the damage growth characteristics of the baseline panel configuration which evolved from the results of Phase I of the program. As a parallel effort to the baseline panel tests, the enhanced panel test program was developed in order to evaluate an enhanced panel design which utilized the Phase I experience, and state-of-the-art damage containment features. These state-of-the-art damage containment features included grid through-stitching of the skins, stitched skin/stiffener interfaces, interleaved stiffener caps, tapered skin flanges, and increased 0-deg planks in the skins under the stiffeners.

The results of the wing structure damage assessment study, the material screening and damage growth coupon tests, the baseline panel tests, and the enhanced panel tests were to feed into the final large compression panel damage tolerance program. Figure 1 presents a schematic of the Phase II program structure showing the progression toward the final large panel design validation tests.

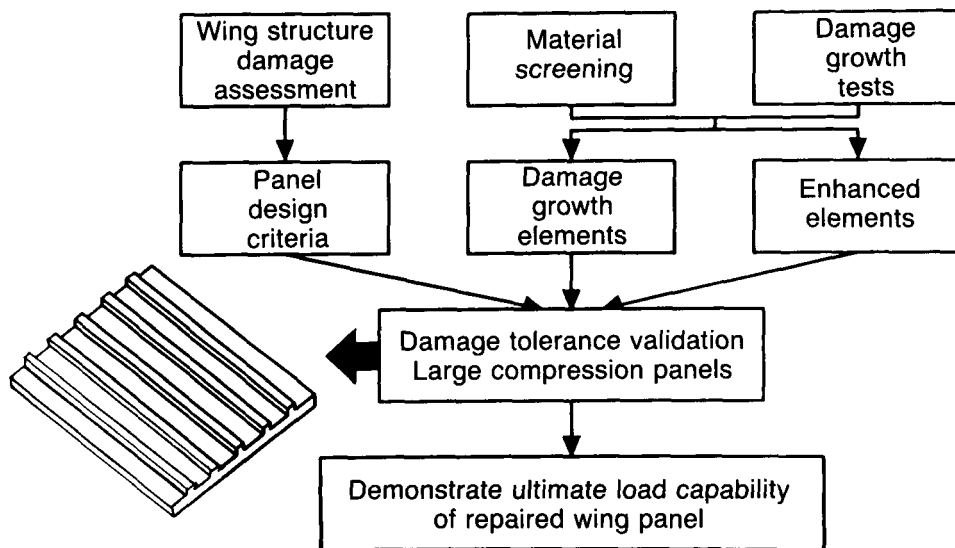


Figure 1. Damage Tolerance Panel Development Program

WING STRUCTURE DAMAGE ASSESSMENT

Because damage is such an important consideration in design, a wing structure damage assessment was performed in order to more fully understand the commercial aircraft wing structure damage environment. The study included investigations into the damage threats, manufacturing and quality control processes, service maintenance and inspection practices, and service histories of commercial airplane wings. The entire study is presented as an appendix, by M. N. Gibbins, P. J. Smith, and R. D. Wilson, to this report.

Boeing has identified four approaches to reducing the negative effects of damage: (1) develop damage tolerant structure, (2) improve quality control to reduce critical manufacturing and fabrication damage, (3) improve non-destructive evaluation (NDE) methods for detecting damage during manufacturing, and (4) develop in-service inspection techniques ensuring that critical service damage is identified.

MATERIAL SCREENING TESTS

As a part of the development of more damage tolerant wing structure, several candidate toughened material systems were selected for evaluation in a material screening test program. NASA standard tests per reference 2 were used to evaluate these materials. These standardized tests (fig. 2) were mutually agreed upon by NASA, Boeing, Douglas, and Lockheed for use in the wing key technology contracts.

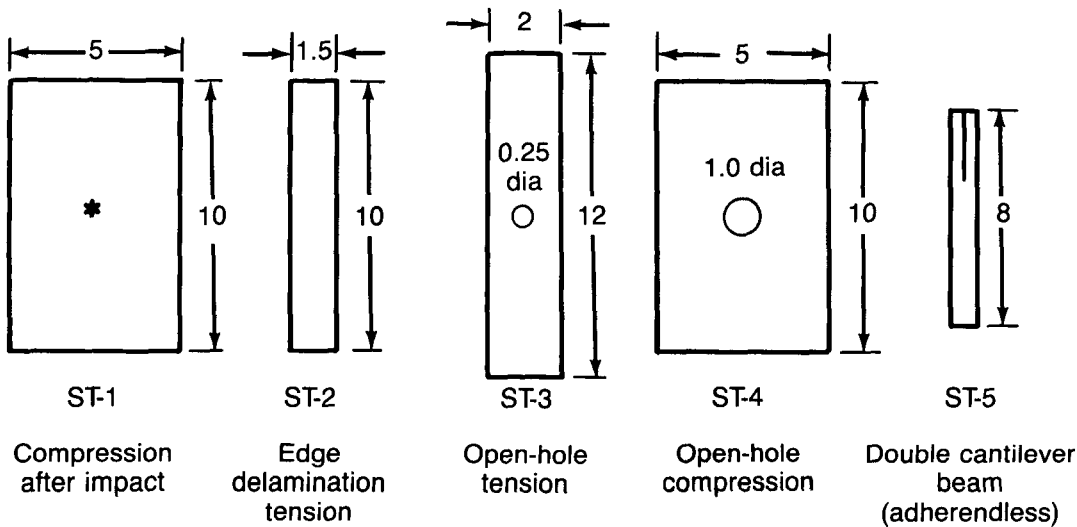


Figure 2. Standard Material Screening Tests

The material systems selected for this screening program were the toughened thermosets AS6/2220-3, AS6/5245C, and AS4/5245C. These materials were obtained in the form of 12-in wide epoxy impregnated graphite unidirectional tape with a nominal resin content of 34%. The AS6/2220-3 and AS6/5245C materials contained graphite with an areal weight of 190 grams/meter² and the AS4/5245C had 145 grams/meter². Also selected for evaluation was the thermoplastic AS4/PEEK, which was obtained in consolidated laminate form. This material system consisted of the APC-2 resin with a nominal 34% content, and an areal graphite weight of 145 grams/meter². Figures 3, 4, and 5 present the results of three of the standard tests. Included for comparison are the results of similar tests performed during Phase 1 on the AS4/2220-3 material.

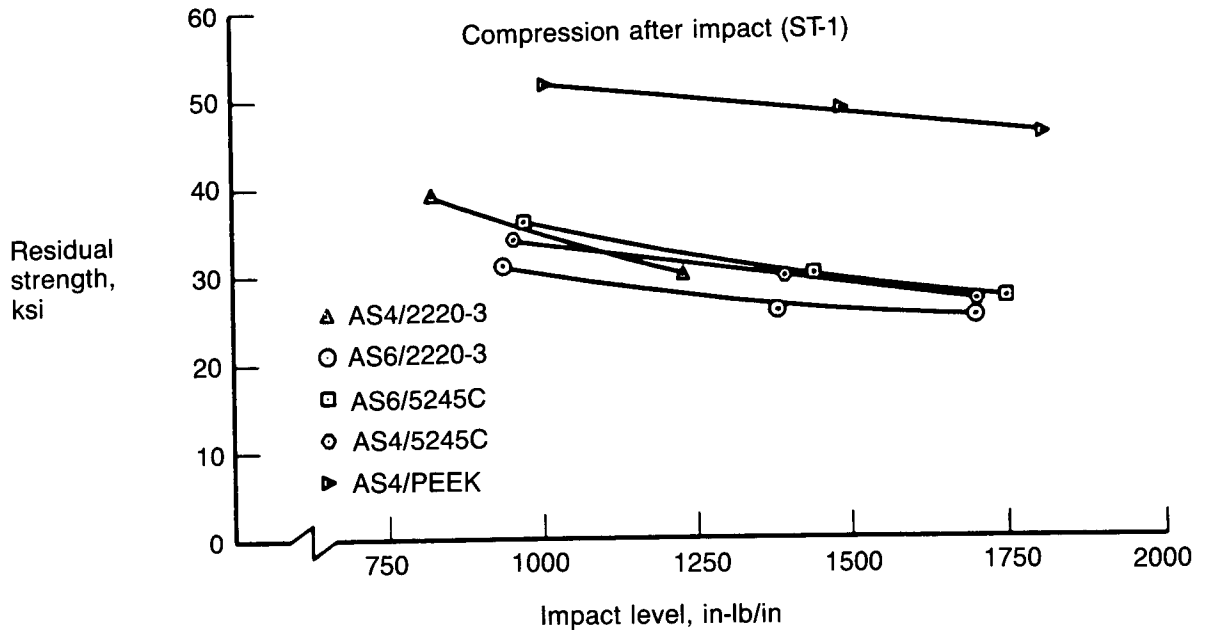


Figure 3. Compression After Impact Test Results

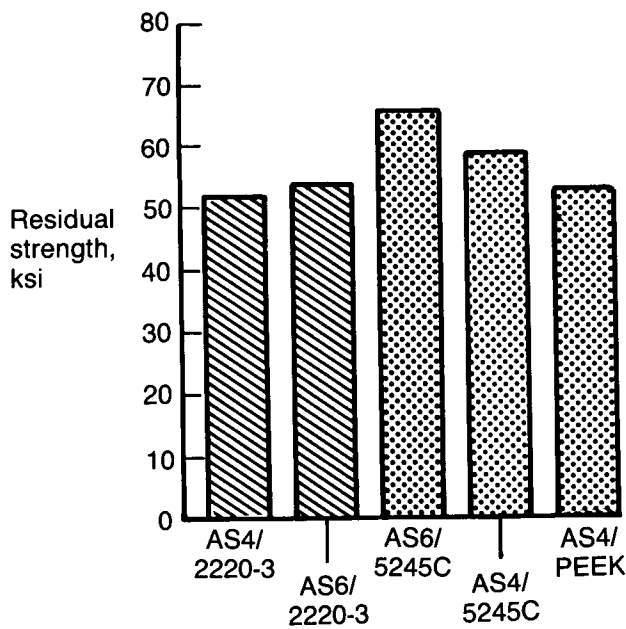


Figure 4. Open Hole Tension (ST-3) Test Results

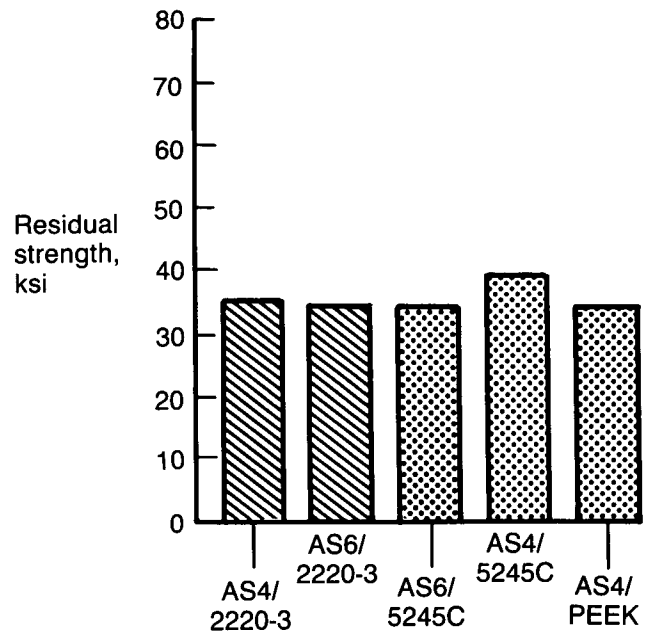


Figure 5. Open Hole Compression (ST-4) Test Results

Figures 6 and 7 present the results of the adherendless double cantilever beam (DCB) (ST-5) tests performed on the AS6/2220-3, AS6/5245C, and AS4/PEEK materials only.

Edge delamination tests (ST-2 of ref. 2) were also performed on the AS6/2220-3, AS6/5245, and AS4/PEEK materials. The G_{IC} values obtained from these tests are mixed-mode material fracture toughness measurements determined as a continuous function of G_{II}/G_I ratio. Experimental evidence (ref. 3) indicated that G_{IC} cannot be accurately determined from mixed-mode energy release rate ($G_{(I,II)}$) as a function of G_{II}/G_I ratio.

Due to this inaccuracy and the difficulties encountered at Boeing in establishing the onset of delaminations, the results of the edge delamination tests have been omitted from this document.

The material screening test program also included basic material property tests for E_{11} and E_{22} in tension and compression, γ_{12} and G_{12} for each material. The results of these tests are presented in Tables 1, 2, 3, 4, and 5. The averaged values obtained for each material were used where applicable in laminate analyses for the panel designs of the basic configuration damage growth panels, the enhanced panels, and the five-stiffener damage tolerance panels.

The performance of the thermoplastic AS4/PEEK was significantly better than any of the thermoset materials in the toughness characteristic tests, and was similar to those of the other materials in the notch strength tests. Of the thermoset materials, the overall performance of the AS6/5245C was marginally better than that of the others.

The AS4/PEEK would have been an obvious choice for use in fabrication of the final five-stiffener damage tolerance panels based on the results of the material screening program. However, the late availability of the PEEK material and the considerable problems associated with the processing and consolidation of this material at the very high curing temperature of 700°F eliminated it from use in the large panel fabrication. Based on its better performance in the compression after impact tests and the G_{IC} fracture toughness tests, the AS6/5245C was chosen to be used in the fabrication of the five-stiffener damage tolerance panels. The AS6/2220-3 material had to be chosen at the onset of Phase II to be the baseline material for the damage growth coupon program, the damage growth test panels, and the enhanced panel test program.

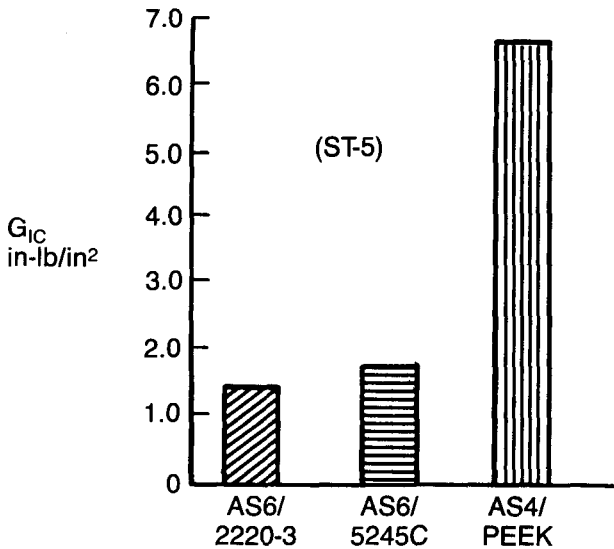


Figure 6. Mode I Fracture Toughness Test Results

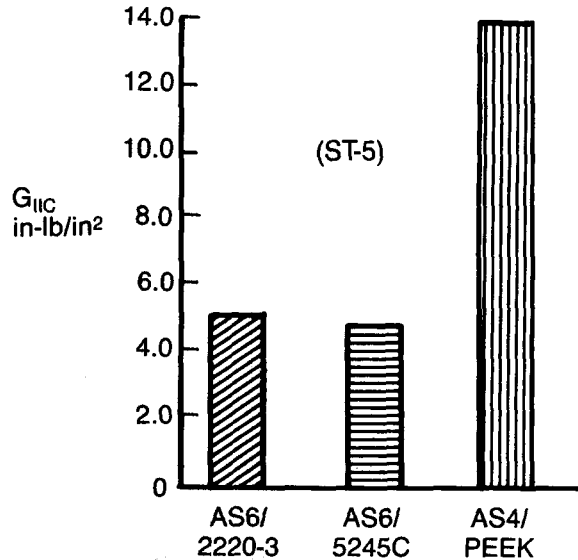


Figure 7. Mode II Fracture Toughness Test Results

Table 1. 0-deg Tension Modulus (E_{11}) and Poisson's Ratio (ν_{12})

Material system	Layup, (deg)	Specimen ID	Test temp, °F	Test environment	E_{11} , msi 1	ν_{12}	Instru- menta- tion
AS6/2220-3 <hr/> Average	[0] ₈ 2	MPT-1A-1 MPT-1A-2 MPT-1A-3	RT	Dry	19.17	.325	'T' strain gage
					20.34	.342	
					20.38	.308	
					20.16	.325	
AS6/5245 <hr/> Average	[0] ₈ 2	MPT-2A-1 MPT-2A-2 MPT-2A-3	RT	Dry	19.73	.300	'T' strain gage
					19.83	.275	
					19.27	.308	
					19.61	.294	
AS4/PEEK <hr/> Average	[0] ₂₀ 3	MPT-4A-1 MPT-4A-2 MPT-4A-3	RT	Dry	18.57	.33	'T' strain gage
					18.74	.33	
					18.55	.38	
					18.72	.35	

- 1 All values normalized to 34% resin content
 2 190 g/m² areal weight of graphite
 3 145 g/m² areal weight of graphite

Table 2. 90-deg Tension Modulus (E_{22})

Material system	Layup, (deg)	Specimen ID	Test temp, °F	Test environment	E_{22} , msi 1		Instru- menta- tion
AS6/2220-3 <hr/> Average	[90] ₈ 2	MPT-1B-1 MPT-1B-2 MPT-1B-3	RT	Dry	1.31		Axial strain gage
					1.25		
					1.19		
					1.25		
AS6/5245 <hr/> Average	[90] ₈ 2	MPT-2B-1 MPT-2B-2 MPT-2B-3	RT	Dry	1.22		Axial strain gage
					1.20		
					1.19		
					1.21		
AS4/PEEK <hr/> Average	[90] ₂₀ 3	MPT-4B-1 MPT-4B-2 MPT-4B-3	RT	Dry	1.42		Axial strain gage
					1.41		
					1.38		
					1.40		

- 1 All values normalized to 34% resin content
 2 190 g/m² areal weight of graphite
 3 145 g/m² areal weight of graphite

Table 3. 45-deg Tension—Shear Modulus (G_{12})

Material system	Layup, (deg)	Specimen ID	Test temp, °F	Test environment	G_{12} , msi 	Instrumentation
AS6/2220-3 Average	[+45/-45] _{2S} 	MPT-1C-1 MPT-1C-2 MPT-1C-3	RT	Dry	.41 .43 .42 .42	'T' strain gage
AS6/5245 Average	[+45/-45] _{2S} 	MPT-2C-1 MPT-2C-2 MPT-2C-3	RT	Dry	.46 .47 .47 .47	'T' strain gage
AS4/PEEK Average	[+45/-45] _{2S} 	MPT-4C-1 MPT-4C-2 MPT-4C-3	RT	Dry	.40 .41 .42 .41	'T' strain gage

-  All values normalized to 34% resin content
-  190 g/m² areal weight of graphite
-  145 g/m² areal weight of graphite

Table 4. 0-deg Compression Modulus (E_{11})

Material system	Layup, (deg)	Specimen ID	Test temp, °F	Test environment	E_{11} , msi 	Instrumentation
AS6/2220-3 Average	[0] ₈ 	MPC-1A-1 MPC-1A-2 MPC-1A-3	RT	Dry	18.27 18.81 19.35 18.81	Axial strain gage
AS6/5245 Average	[0] ₈ 	MPC-2A-1 MPC-2A-2 MPC-2A-3	RT	Dry	21.62 18.64 15.83 18.70	Axial strain gage
AS4/PEEK Average	[0] ₂₀ 	MPC-4A-1 MPC-4A-2 MPC-4A-3	RT	Dry	15.80 16.15 15.76 15.90	Axial strain gage

-  All values normalized to 34% resin content
-  190 g/m² areal weight of graphite
-  145 g/m² areal weight of graphite

Table 5. 90-deg Compression Modulus (E_{22})

Material system	Layup, (deg)	Specimen ID	Test temp, °F	Test environment	E_{22} , msi 	Instrumentation
AS6/2220-3 <hr/> Average	[90] ₈ 	MPC-1B-1 MPC-1B-2 MPC-1B-3	RT	Dry	1.35	Axial strain gage
					1.38	
					1.52	
					1.42	
AS6/5245 <hr/> Average	[90] ₈ 	MPC-2B-1 MPC-2B-2 MPC-2B-3	RT	Dry	1.46	Axial strain gage
					1.43	
					1.36	
					1.42	
AS4/PEEK <hr/> Average	[90] ₂₀ 	MPC-4B-1 MPC-4B-2 MPC-4B-3	RT	Dry	1.54	Axial strain gage
					1.57	
					1.55	
					1.55	

-  All values normalized to 34% resin content
-  190 g/m² areal weight of graphite
-  145 g/m² areal weight of graphite

DAMAGE GROWTH COUPON TESTS

The toughened thermoset material, AS6/2220-3, was chosen as the Phase II baseline material for damage growth evaluations at both coupon and panel level. The purpose of the damage growth coupon test program was to evaluate the damage growth characteristics of low velocity impact damaged coupons after load cycling. The test program included five types of known initial damage, two fatigue environments, various different strain levels, and utilized the compression-after-impact coupon ST-4 (ref. fig. 2). The five types of known initial damage were: delaminations from 280 in-lb of impact energy; delaminations from 500 in-lb of impact energy; open hole with delamination damage; delaminations from 500 in-lb of impact energy in through-stitched laminates (Kevlar stitches in rows of four stitches/inch at both .25-in and .05-in row spacing); and multiple delamination simulation of impact damage, using nine Teflon discs of varying sizes inserted between plies in a cone-shaped arrangement through the laminate thickness. The configuration of the simulated multiple delamination specimen is presented in Figure 8.

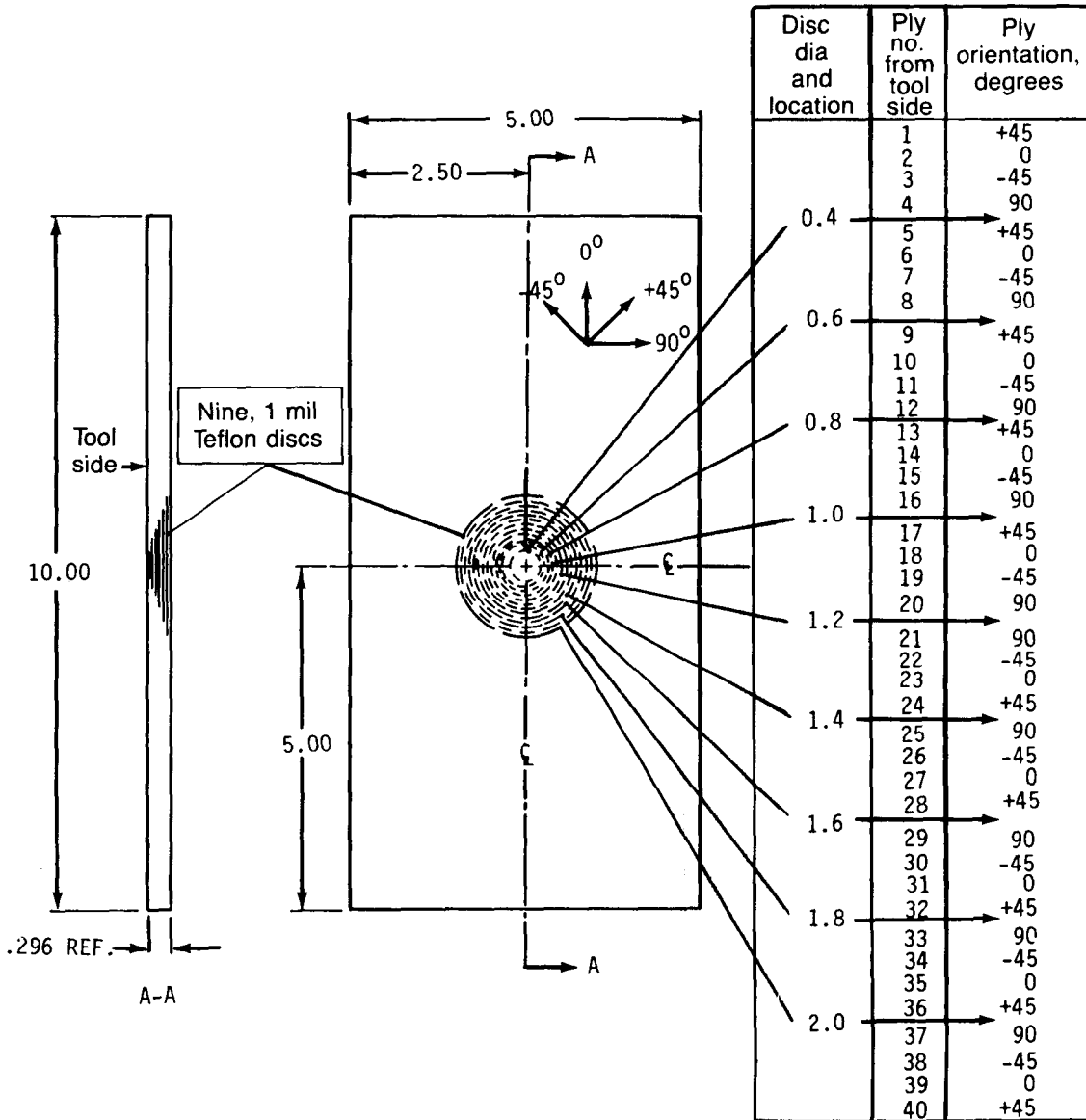


Figure 8. Simulated Impact Multidelamination Specimen Configuration

The fatigue environments were (a) constant amplitude compression-compression load cycling ($R=10.0$), and (b) spectrum fatigue load cycling based on the Boeing 767 airplane wing upper surface cyclic fatigue spectrum with the tension load excursions replaced by small compression loads. This removal of the tension loads was done in order to facilitate testing with the standard compression-after-impact specimen and test jig. The work done by Byers (ref. 4) showed that compression-compression fatigue was a severe fatigue environment for delamination damaged laminates, and Boeing IR&D efforts have indicated that compression-compression ($R=10.0$) is generally as severe as tension-compression ($R=-2.0$) for a quasi-isotropic laminate with damage.

The full Boeing 767 cyclic spectrum was made up of 163,971 total load cycles for a block of 5000 flights containing five different flights. Twelve blocks of 5000 flights made up a lifetime for a total of 1,967,652 load cycles. In order to speed testing, the spectrum was truncated by retaining only the maximum load cycle from each flight so that the truncated spectrum consisted of 60,000 cycles. The truncated spectrum was checked against the full spectrum on stitched specimens containing 500 in-lb impact damage and no detectable difference in fatigue performance was found.

The maximum strain levels used during the damage growth cycling were selected based on the static strength of each damage type. For the constant amplitude ($R=10.0$) cycling, the strains at maximum cyclic load (P_{min}) were 60%, 65%, 70% up to 75% of those strains of the static strength (P_{ult}) of each damage type. For the spectrum fatigue cycling, the strains at the maximum load excursions (P_{min} cyclic) were 65%, 70%, 80%, 85%, and 90% of the strains at P_{ult} of each damage type. For all of the damage types, it was found that the constant amplitude cycling was much more detrimental to the delaminated laminates than the spectrum cycling. This can be seen in Figure 9 which presents the two fatigue environmental effects on specimens with similar damage types. The residual strength of the spectrum cycled specimen with seven total lifetimes of load cycling up to P_{min} cyclic/ $P_{ult} = 90\%$ was almost that of the constant amplitude cycled specimens with four lifetimes of load cycling up to $P_{min}/P_{ult} = 70\%$.

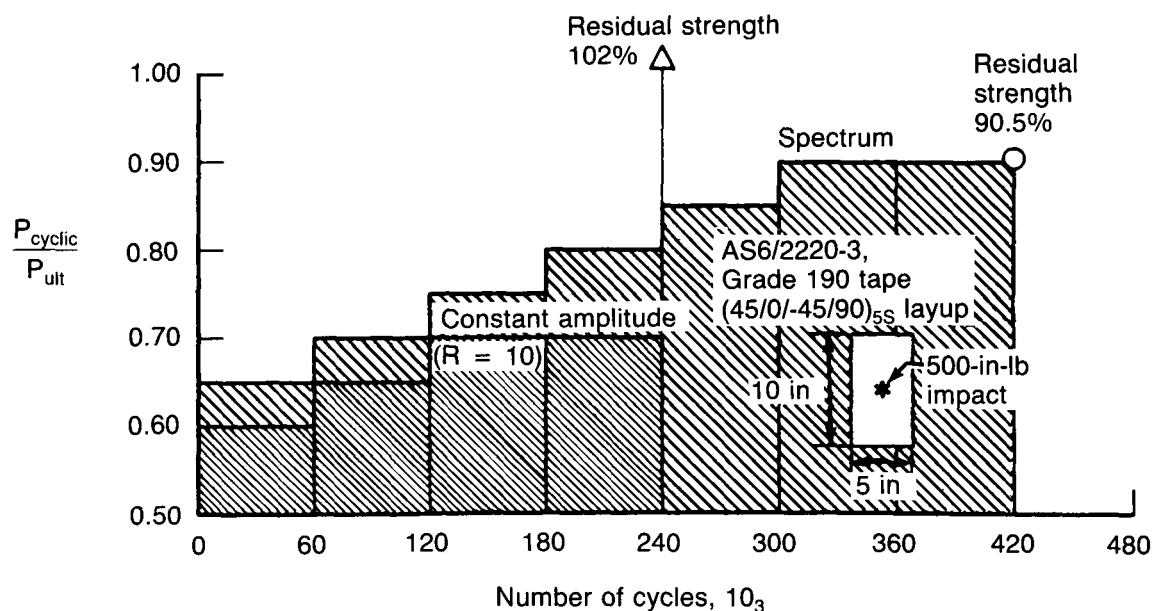


Figure 9. Fatigue Performance of 500-in-lb Impact Damaged Coupons

Periodic inspections utilizing through-transmission (TTU) NDE equipment monitored the damage growth. If damage growth had not been detected for a particular strain level after 60,000 cycles (one lifetime of the truncated 767 cyclic spectrum), the strain level was increased 5% and monitored again for damage growth up to 60,000 cycles. This procedure was repeated until damage growth was detected, then the damage growth characteristics were monitored for one lifetime for each strain level until two-piece failure, or testing was discontinued and the specimen tested statically to determine the residual strength.

In general, little or no damage growth was detected for those specimens subjected to the spectrum fatigue, even at maximum cyclic loads up to 80% of P_{max} . Of the specimens cycled at constant amplitude fatigue, only those specimens containing simulated delaminations and delamination damage around a 1.0-in diameter open hole displayed significant internal damage growth. Figures 10 and 11 present the results of constant amplitude cycling on both damage types. Even on these damage types, the strain levels that promoted damage growth were 65% and 70% of the ultimate strains for those damage types. The constant amplitude strain that grew damage for the specimen with delaminations around the 1.0-in diameter hole was 0.0028 and that for the simulated impact damaged specimen was 0.0024. The maximum load, which occurs once every 5000 flights in the 767 cyclic fatigue spectrum, is equivalent to 0.0029 strain for an upper wing surface designed to 0.006 ultimate strain. The only damage type which exhibited damage growth strain below this level for spectrum fatigue cycling was the simulated delamination specimen. This specimen was designed to simulate an impact damage of 280 in-lb energy, but when tested uncycled, demonstrated only 76% of the static strength of an uncycled specimen with 280 in-lb of impact damage, indicating that it is not representative of typical impact damage.

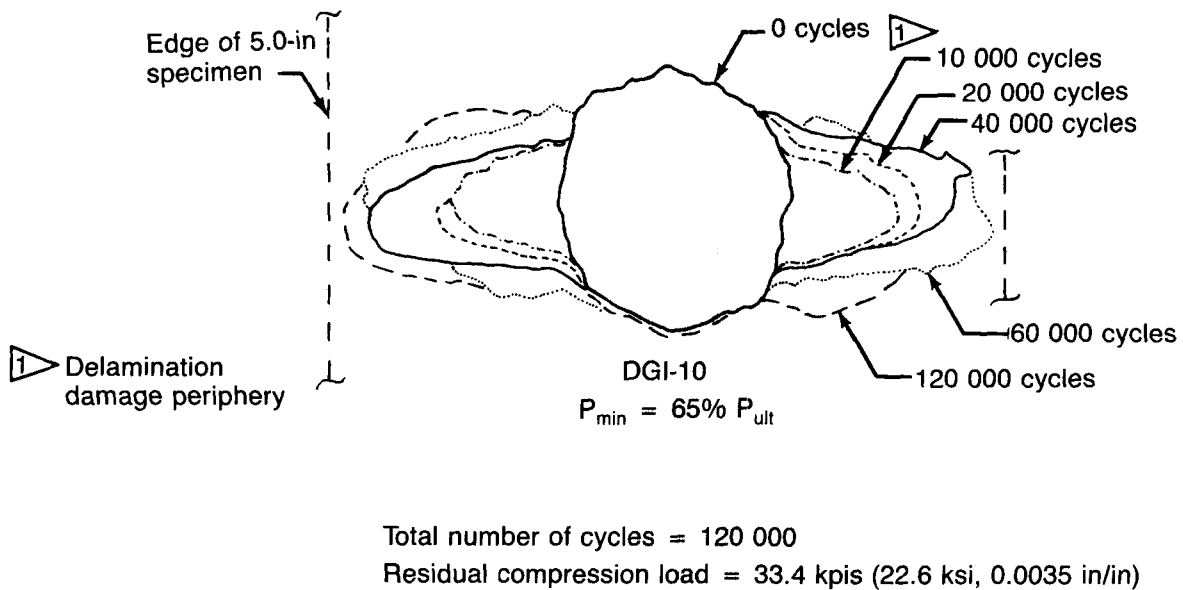


Figure 10. Damage Growth of 280-in-lb Impact-Damaged Specimen Subjected to Constant Amplitude ($R = 10.0$) Cycling

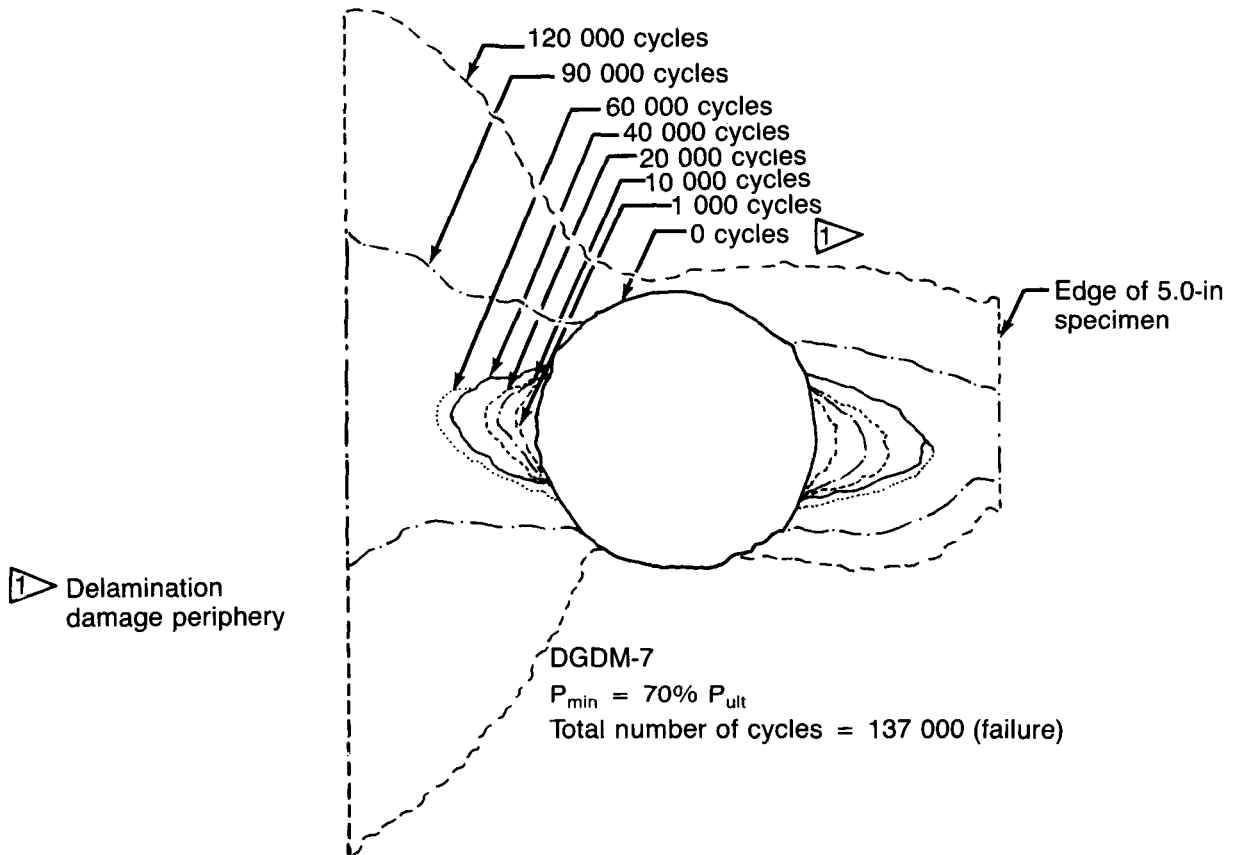


Figure 11. Damage Growth of Simulated Multiple Delamination Specimen Subjected to Constant Amplitude ($R = 10.0$) Cycling

Figure 12 presents the constant amplitude fatigue performance of the damage types tested showing fatigue endurance runout at about 70% of the static strengths. Figure 13 presents the residual static compression strength of all of the damage types for both uncycled and cycled specimens. The fatigue loaded specimens had all been cycled for several lifetimes and their residual compression strengths had degraded very little from the uncycled strengths. The specimens with Kevlar stitches at 0.25 row spacing which had been subjected to 500 in-lb impact damage exhibited the best static and fatigue compression after impact strength.

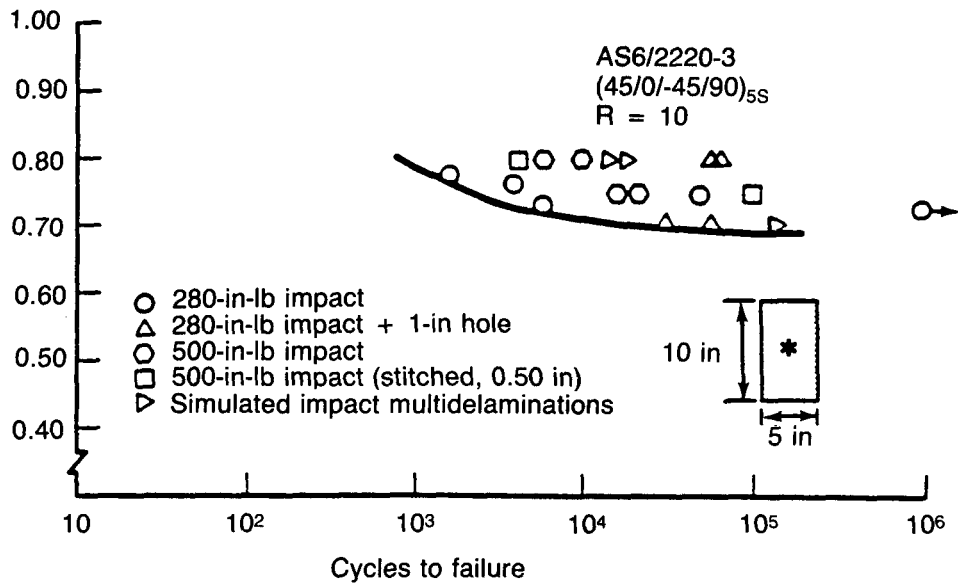


Figure 12. Fatigue Performance of Impact Damaged Coupons

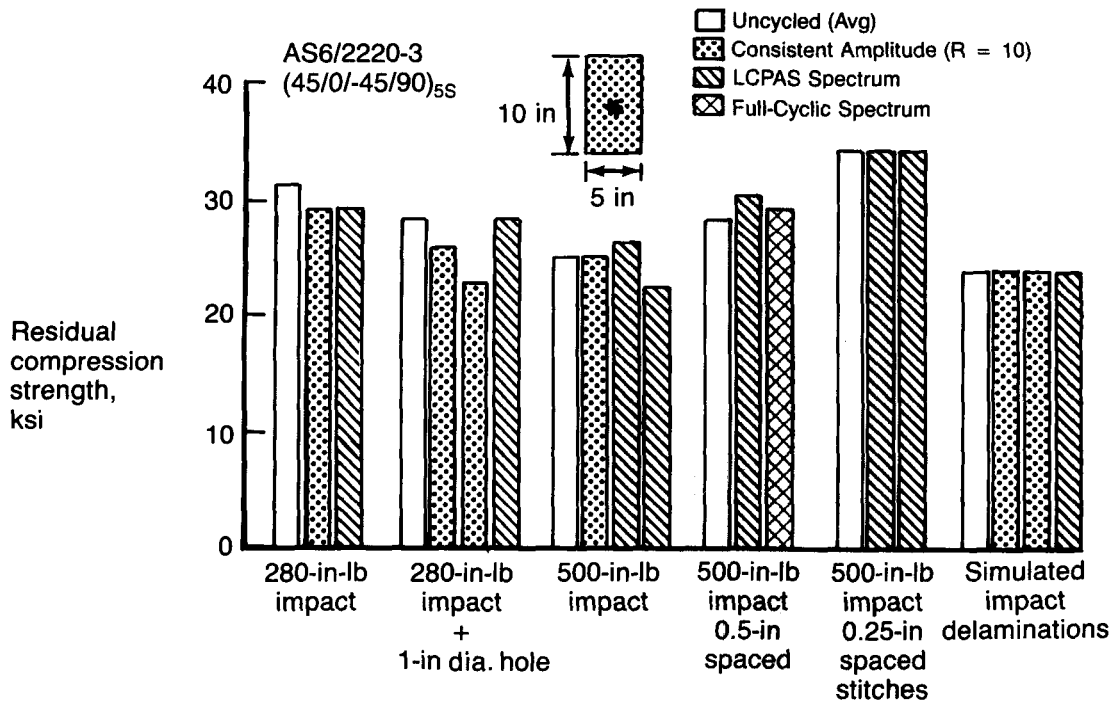


Figure 13. Residual Compression Strength of Impact Conditioned Specimens After Fatigue Cycling

DAMAGE GROWTH ELEMENT TESTS

Further Phase II damage growth testing was performed on three-stiffener panels in order to evaluate the damage growth characteristics of the baseline panel configuration which had evolved from the results of Phase I of the program. The baseline panels were fabricated from AS6/2220-3 material and utilized the damage tolerant soft skin of (10/80/10)%, with discrete 0-deg planks embedded in the skin under the stiffeners, and relatively hard stiffeners ($E=12.5 \times 10^6$ psi) which carry 50% of the total panel end load. Figure 14 presents a cross-section of the baseline panel design. The overall panel extensional modulus was 8.5×10^6 psi which produces 52.4 KSI stress and .0062 strain at the design ultimate end load of 30 kips/inch. The panel torsional shear stiffness (Gt) was 1207 kips/in.

The critical impact locations highlighted in the wing damage study were addressed in this test program. These impact locations and energy levels are presented in Figure 14. The skin impact damages (A) and (C) were not easily visible with impact dents in the laminate surfaces of approximately 0.03 inch. The stiffener cap impact (B) was more visible with a larger dent, approximately .06-in deep.

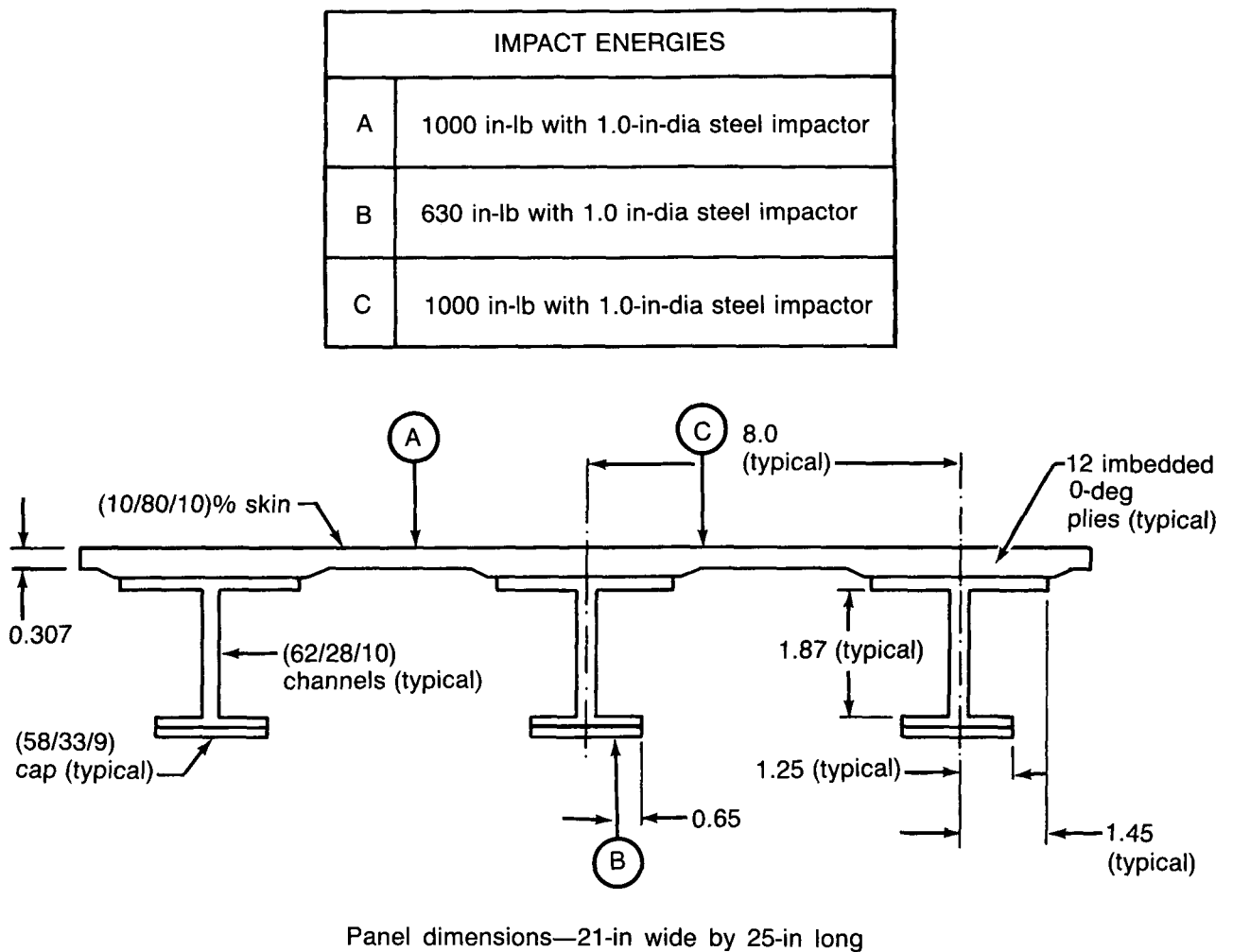


Figure 14. Baseline Panel Configuration and Impact Locations

The first panel, 65C2390-1, was impacted on the skin at the panel centerline between stiffeners at location (A) with 1000 in-lb of energy and tested to static compression failure. The panel failed through the impact damage at a load of 680 kips representing an average gross area panel segment stress of 51.5 KSI and an average P/AE strain of .00605 in/in.

The second panel, 65C23890-2, was also impact damaged on the skin between stiffeners at location (A) with 1000 in-lb of energy and cycled in spectrum fatigue. The fatigue spectrum used was the same as the one used in the damage growth coupon tests with the maximum cyclic load (P_{min}) in the spectrum set at 340 kips. This load represented 50% of the static compression failure load and was equivalent to 0.003 strain. The panel was cycled for two lifetimes (120,000 cycles) of the truncated spectrum loading with periodic pulse echo inspections in order to monitor damage growth. A limit load ($P_{LIMIT}=450$ kips) survey was made after each lifetime (60,000 cycles). Small damage growth was detected after 20,000 cycles, but nothing more was discovered through 120,000 cycles.

The fatigue loading was then changed to constant amplitude cycling ($R=10.0$) with the maximum cyclic load (P_{min}) set at 400 kips. This represented 60% of P_{ult} and a P/AE strain of 0.0035. After 20,000 cycles, no damage growth was detected so the cyclic loading was increased to P_{min} equal to 440 kips (65% of P_{ult} and P/AE strain of .0039. After 10,000 load cycles at this level, the pulse echo inspection detected no damage growth so the load level was increased again, such that P_{min} was equal to 476 kips (70% of P_{ult} and P/AE strain of .0042).

After 5000 cycles, the panel was reinspected and again no damage growth was detected. The maximum cyclic loading was increased to P_{min} equal to 495 kips (73% of P_{ult} and P/AE strain of .0044). This time damage growth was detected after 10,000 cycles. The load cycling was continued and another inspection performed after 10,000 additional cycles. No damage growth was detected and the cycling was continued again. The panel failed through the damage after 9660 additional cycles at $P_{min}=.73 P_{ult}$. Figure 15 presents the damage growth and initial impact damage size for this panel.

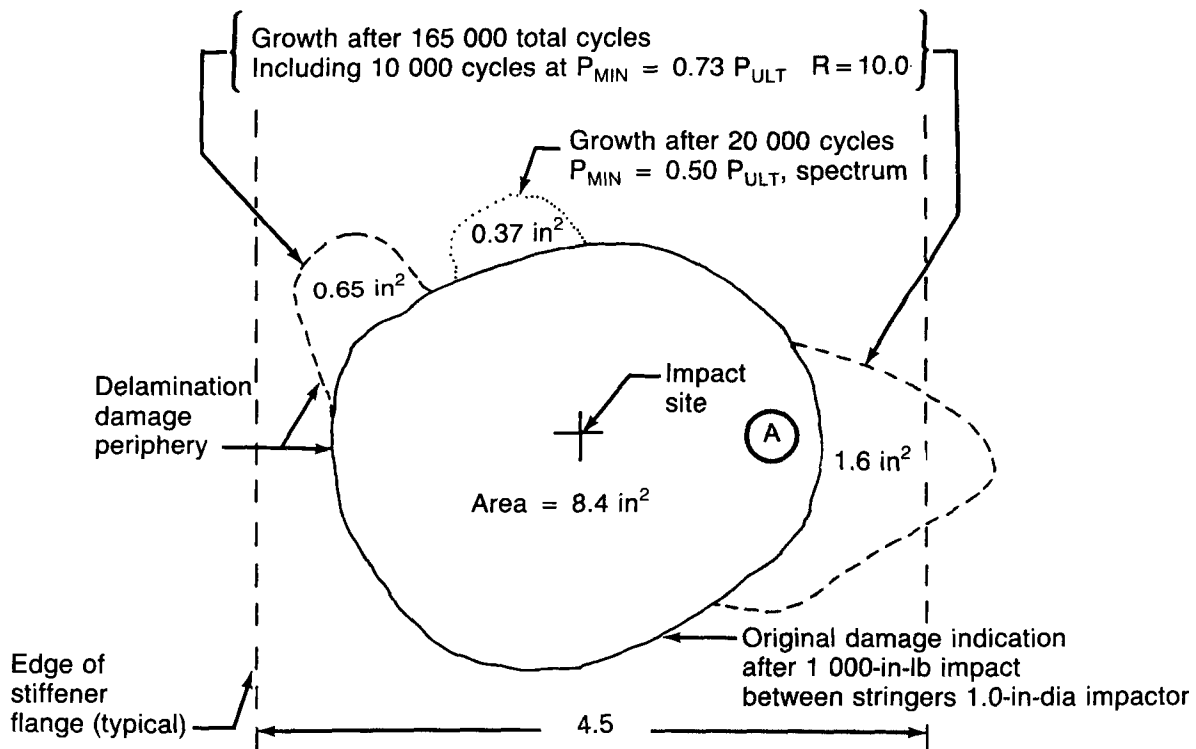


Figure 15. Damage Growth Results of Fatigue Cycling of Impact Damage Panel 65C23890-2

The third baseline panel, 65C23890-3, was impacted on the central stiffener cap at location (B) (ref. fig. 11) with 630 in-lb of energy. This impact level had been determined to produce barely visible stiffener cap damage from the results of a Boeing IR&D studies, but the actual damage incurred was easily visible. The panel was cycled in spectrum fatigue for two lifetimes (120,000 cycles) and two limit load surveys without any damage growth detected during periodic pulse echo inspections. The maximum cyclic load (P_{min}) was 340 kips (50% of P_{ult} at P/AE strain of .0030). The panel was then removed from the test machine, impacted on the skin at the panel centerline at location (A) (ref. fig. 14) with 1000 in-lb of energy. The panel was then spectrum cycled to one more lifetime with P_{min} equal to 50% of P_{ult} . No damage growth at either damage site was observed during the periodic pulse echo inspections. The panel was then being loaded to limit load (450 kips) when two-piece failure occurred at 430 kips (96% of design limit load and P/AE strain of 0.0038). The failure occurred at the center of the panel through both damage sites. The NDE history for panel 65C23890-3 is presented in Figure 16.

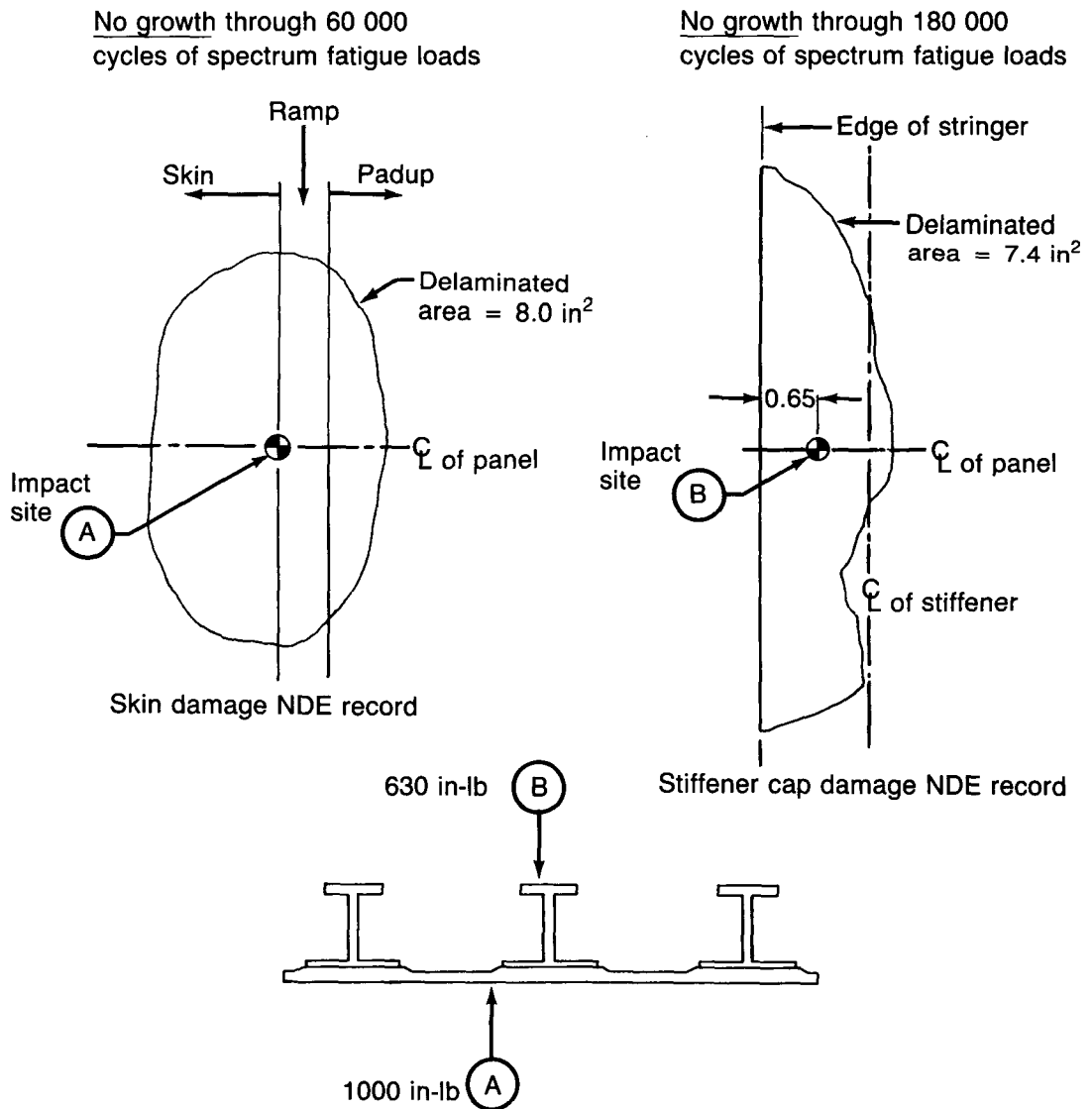


Figure 16. Damage Growth Results of Fatigue Cycling of Impact Damaged Panel 65C23890-3

The results of the baseline panel damage growth test program are presented in Table 6. The general conclusions of this program are that typically commercial airplane spectrum fatigue cycling does not cause damage growth in impact damaged upper wing surface compression panels.

Table 6. Baseline Panel Damage Growth Test Results

Panel no.	Impact damage (1-in-dia impactor)	Impact location	Failure load (kips)	Average segment stress (ksi)	Average P/AE strain (in/in)	Fatigue load cycles
65C23890-1	1000 in-lb	On skin-between stiffeners	-680	-51.5	-0.00605	--
65C23890-2	1000 in-lb	On skin-between stiffeners	 -495	-37.5	-0.00441	185 000
65C23980-3	630 in-lb	On stringer cap	 -430	-32.5	-0.00383	180 000
	1000 in-lb	On skin-at padup ramp				

-  Failed during fatigue load cycling after 185 000 cycles (over three equivalent lifelines)
-  Failed after 180 000 spectrum fatigue cycles during a limit load test

ENHANCED DESIGN PANELS

The enhanced panel design was developed from the experience gained from the Phase 1 panel tests, the Phase II damage growth coupon study, and state-of-the-art damage containment concepts. The design features are shown in Figures 17 and 18. The soft skin had continued to demonstrate good damage tolerance, and the damage growth coupon tests demonstrated improved damage containment and residual compression strength from through-stitching of prepreg laminates. The wing structure damage assessment study highlighted the criticality of the stiffener cap, and therefore, interleaving of the 0-deg plies with 45-deg plies was accomplished to increase the damage tolerance of the stiffener cap. The interleaved stiffener cap allowed for a slimmer stiffener web and for more 0-deg planks to be buried in the skin for greater damage containment. Ply layouts for the various panel elements are shown in Table 7.

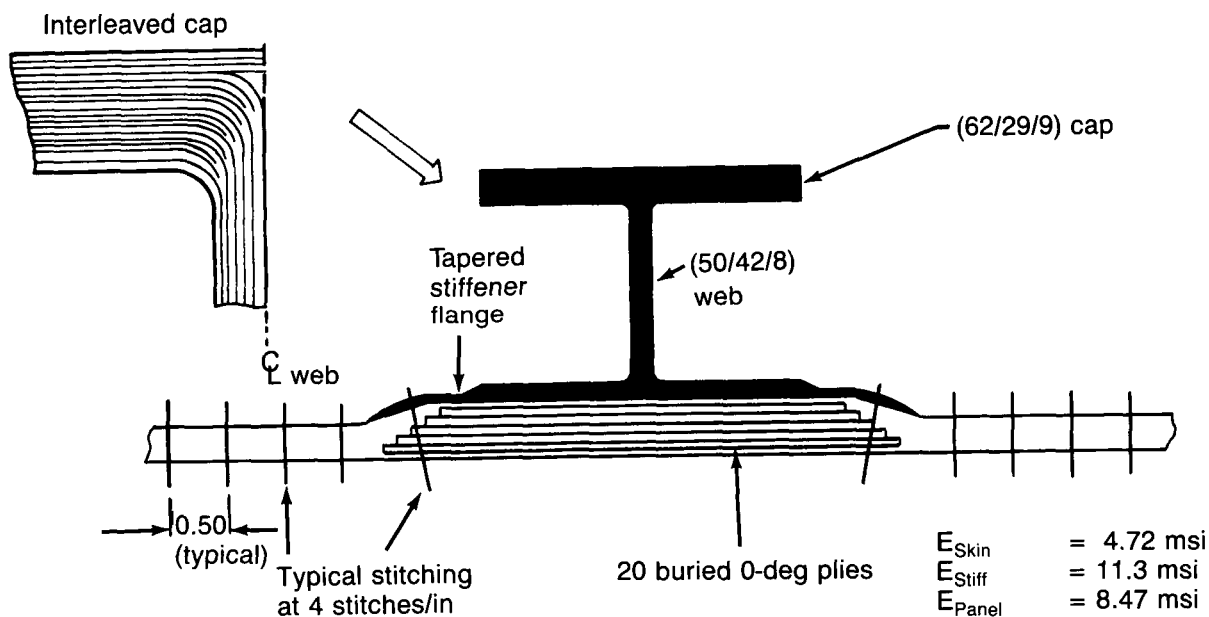


Figure 17. Enhanced Stiffened Panel Design Features

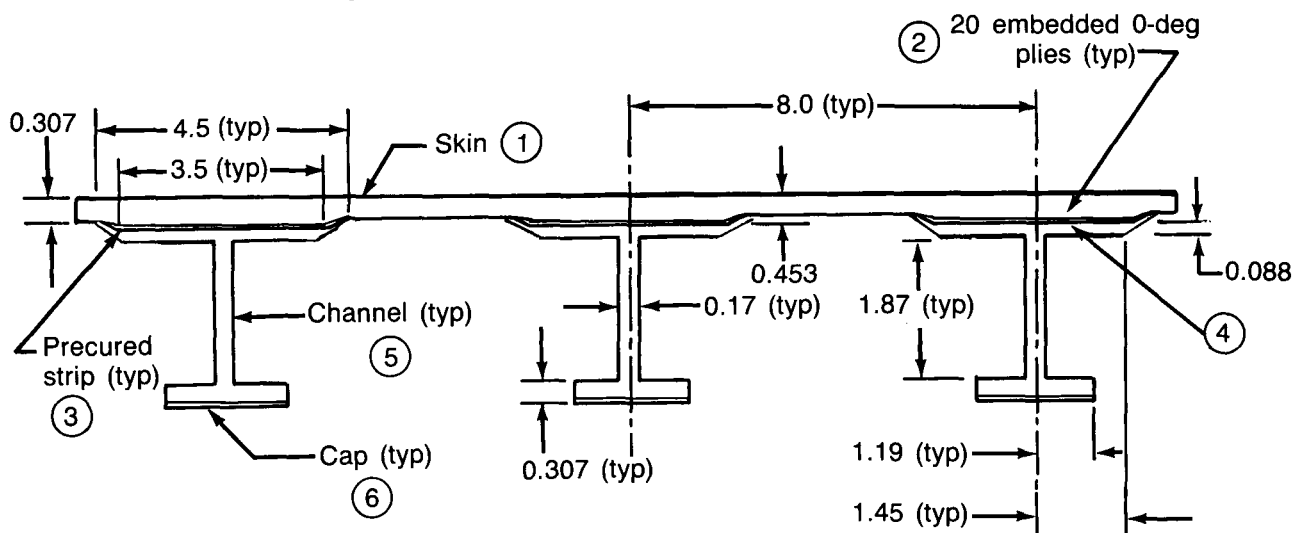


Figure 18. Enhanced Panel Configuration

The skin-stiffener interface, which is cocured and contains a precured strip (fig. 18), is a critical location for panel failure initiation. Through-stitching of this detail with Kevlar yarn was done to enhance this interface. The skin flanges of the stiffener were tapered down in thickness and lengthened to drape over the skin pad-up ramps in order to allow skin-stiffener flange stitching while stiffener tools were in place. This feature was also judged to provide for greater durability than the conventional nontapered stiffener skin flange of the baseline design. Because of manufacturing constraints, the skin through-stitching was performed in rows 0.50-in apart rather than the optimum 0.25-in spacing of the damage growth coupon tests.

Three-stiffener test panels were fabricated from AS6/2220-3 material to provide a direct design comparison with the baseline three-stiffener panel tests. Stiffener spacing and panel dimensions were identical. The test program included three panels tested in static compression to determine the damage tolerance of the enhanced design. The baseline damage growth panel test program had shown that durability was not as critical as damage tolerance. The Phase 1 panel tests had demonstrated that the ultimate load case with barely visible damage was the most critical design case. Figure 19 presents the enhanced panel impact damage locations and energy levels.

Table 7. Enhanced Panel Design Ply Layup

Skin	Skin padup	Precured strip	Stiffener flange	Stiffener web	Stiffener cap
Element 1	Element 2	Element 3	Element 4	Element 5	Element 6
-45	-45	+ 45	± 45	0 ₂	± 45
90	90	0	90	-45	90 ₂
+ 45	+ 45	+ 45	± 45	0 ₄	-45
0	0		0 ₄	∓45	0 ₃
-45	-45		-45	90	+ 45
90	90		0 ₂	∓45	0 ₃
± 45	± 45			Q sym	-45
+ 45	+ 45				0 ₄
∓45 ₄	0 ₄ plank				+ 45
-45	∓45 ₃				0 ₄
0	0 ₄ plank				+ 45
± 45	∓45				0 ₄
Q sym	-45				-45
	0				0 ₄
	± 45				+ 45
	0 ₂ plank				0 ₄
	Q sym				-45
					90 ₂
					∓45

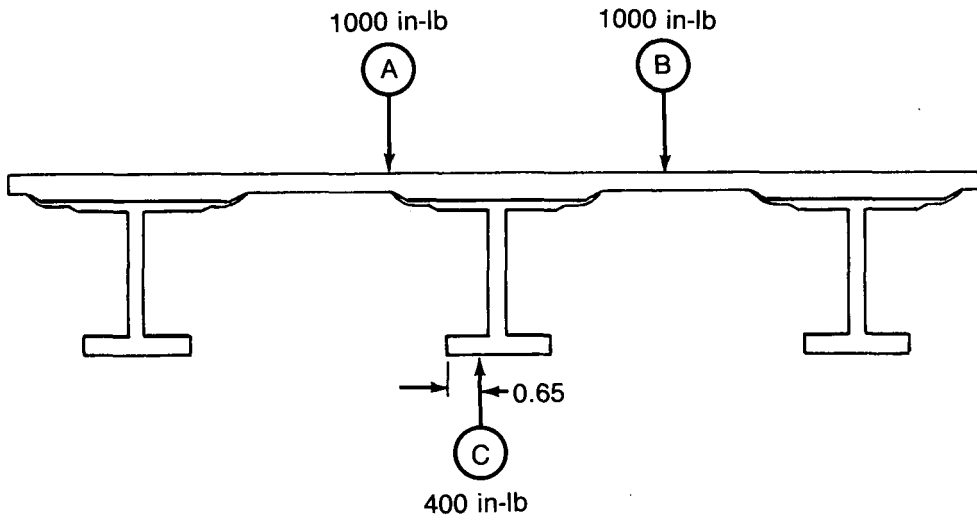


Figure 19. Enhanced Test Program Impact Locations and Energy Levels

The 1000 in-lb impacts to the skins were similar to those of the baseline panel tests. The 650 in-lb impact to the baseline panel stiffener cap had produced damage which was considered greater than barely visible; therefore, the enhanced panel stiffener cap damage was reduced to 400 in-lb. The results of the pulse echo NDE inspections of the skin impacts at location (A) on panel 65C23891-1 and location (B) on panel 65C23891-2 are presented and compared to the results of the baseline panel skin impact inspections in Figure 20. It can be seen that the 0.50-in row spaced grid stitching of the skins significantly reduces the area of delaminations caused by the impacts. Each of the impacts caused barely visible damage and the associated dents were less than 0.05-in deep.

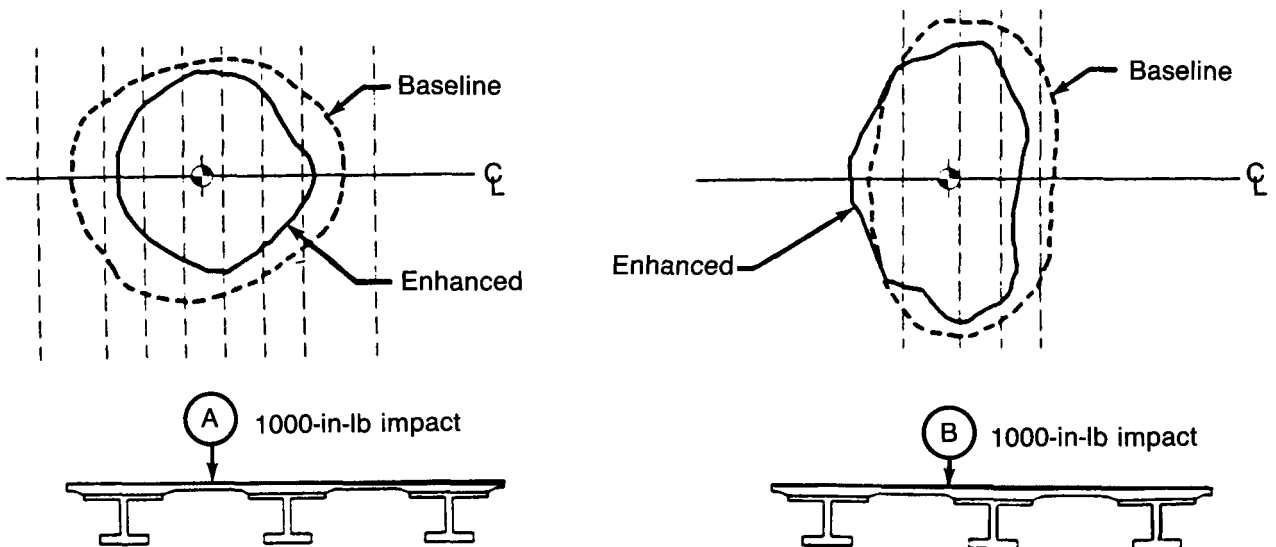


Figure 20. NDE Records of Impact Delaminations, Baseline Versus Enhanced Designs

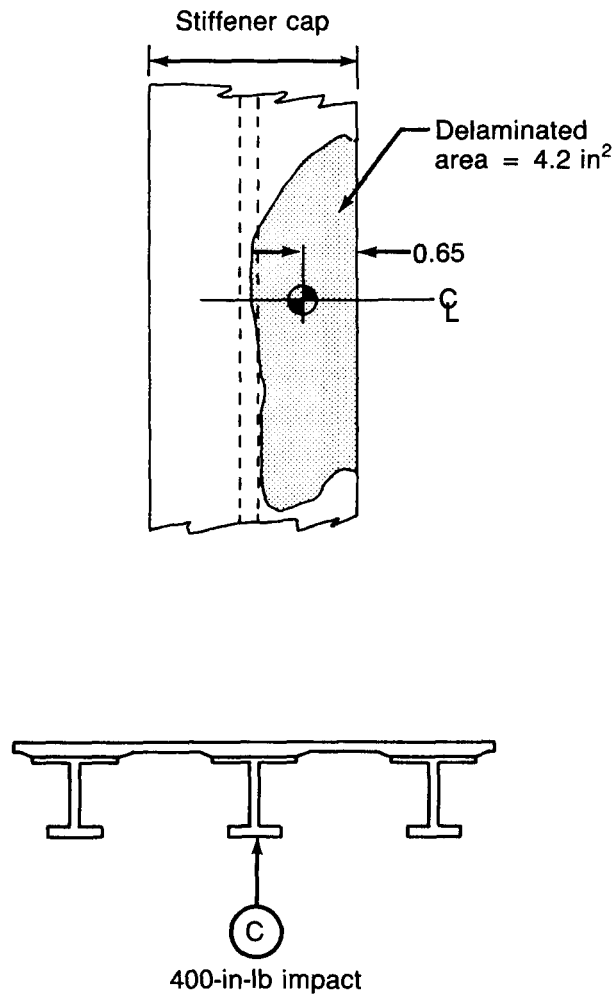


Figure 21. NDE Record of Impact Delaminations in Center Stiffener Cap of Panel 65C23891-3

Figure 21 presents the results of the NDE inspection of the stiffener cap damage of panel 65C23891-3. It can be seen that even the reduced level of impact energy still caused a large area of delaminations in the cap, 4.2 in² compared to 7.4 in² of the baseline 630 in-lb of impact energy.

Each of the panels was tested to two-piece static compression failure. All panels failed through their damage sites. The results of the enhanced panel tests are presented in Table 8. The two panels with the impact damage in the skin yielded an average of 15% greater residual compression strength than the stiffener damaged panel. All three stiffeners were completely detached from the skin after failure of the stiffener damaged panel. The panels with the skin damage did not exhibit this interface failure. Panels 65C23891-2 and 65C23891-3 had NDE indications of voids or cracks and delaminations in the skin flanges of the stiffener adjacent to the precured strips in the skin-stiffener interfaces. Panel 65C23891-3, with the stiffener cap damage, had more of these indications than panel 65C23891-2. The effect of these anomalies on the structural integrity of the panel skin-stiffener interface is not known. The NDE inspections of the five-stiffener panels (ref. fig. 23) revealed considerably more of these anomalies.

Table 8. Test Results of Enhanced Three-Stiffener Panel Program

Panel no.	Impact damage (1-in-dia impactor)	Impact location	Failure load (kips)	Average segment stress (ksi)	Average P/AE strain (in/in)
65C23891-1	1000 in-lb	Ⓐ On skin between stiffeners	-761	-57.7	-0.0068
65C23891-2 1	1000 in-lb	Ⓑ On skin at edge of padup ramp	-744	-56.4	-0.0068
65C23891-3 2	400 in-lb	Ⓒ On stiffener cap	-653.3	-49.6	-0.00585

1 NDI indications of voids or cracks and delaminations in radii of stiffener flanges

2 Increased NDI indications of voids or cracks and delaminations in radii of stiffener flanges

Panel 65C23891-1, with the 1000 in-lb impact on the skin directly between stiffeners, tested 12.4% better than the baseline panel with similar impact damage.

The grid stitching of the enhanced panel skins not only inhibited delamination damage at the impact event, but also contributed to increased residual compression strength. The individual effects of the other panel enhancements are not known, but the total enhanced panel design proved superior to the baseline design.

LARGE PANEL DAMAGE TOLERANCE VALIDATION TESTS

The large panel damage tolerance program tests were performed to validate the final panel design. Four long column five-stiffener panels were tested in static compression to assess the effect of skin and stiffener damage on the ultimate, limit, and safe flight load capabilities of the final upper surface wing panel design. The panels were 37-in wide with five stiffeners and 60-in long to simulate two rib bays. Aluminum ribs were attached to the stiffener caps with C-clamps and the ends of the panels had cobonded doublers and were potted in order to provide stable load introduction. The panel design retained the enhanced panel damage tolerance features with the added feature that the rows of grid stitches in the skins were doubled. This reduced row spacing had demonstrated increased damage containment and residual compression-after-impact strength (ref. fig. 13) during the damage growth coupon test program. Three of the panels retained the skin-stiffener flange stitching of the enhanced panels, and one panel was fabricated without this feature. One other change from the enhanced panels was the selection of AS6/5245C material. This material had demonstrated an 11% increase in compression-after-impact strength (ref. fig. 3) and 20% increase in Mode I fracture toughness (ref. fig. 6) over the AS6/2220-3 baseline material during the material screening tests.

The five-stiffener panel test configuration is presented in Figure 22. The end-potting, cobonded doublers, and simulated ribs are shown together with installed test instrumentation. The instrumentation consisted of axial strain gages to record panel strains, deflectometers to record out-of-plane deflections, and acoustic emission transducers to monitor damage growth. The skin side of the panels was painted with Moire fringe material in order to provide a record of any skin deflections and buckles.

During the fabrication of the five-stiffener panels, a number of material processing problems arose. The AS6/5245C material was difficult to use because of lack of tack and boardiness. These material problems made stiffener ply lay-down on the tools extremely difficult. Each ply was compacted after lay-down as standard practice, but the complete compaction of the stiffeners and skin-stiffener interfaces containing the cobonded precured strip was in doubt. The pulse echo inspection results of the completed panel ① are shown in Figure 23. Panels ②, ③, and ④ had similar, but fewer, pulse echo indications.

End trim from panel ① was sectioned through a number of the pulse echo indicated areas, and photomicrographs were taken. Figure 24 presents a photomicrograph of one of these sections. A number of voids and suspect compaction areas can be clearly noted in the stiffener radius and stiffener-skin interface.

The large panel damage tolerance validation test plan is shown in Table 9. Panels ① and ④ were to demonstrate the ultimate load case with barely visible impact damages. Panels ② and ③ were to demonstrate limit load with easily visible impact damage and then be inflicted with progressive severe damage to evaluate the continued safe flight load capability for panels with and without skin-stiffener flange stitching.

The results of the pulse echo inspections of the impact sites for the 400 in-lb stiffener damage of panel ① and the 2000 in-lb skin damages of panels ② and ③ are presented in Figures 25 and 26. The total area of delamination discovered in the stiffener cap of panel ① after a 400 in-lb impact with a 1.0 diameter steel impactor was larger than of the three-stiffener enhanced stiffener cap after a similar impact (ref. fig. 21). The damage was also more visible with some evidence of the stiffener cap being bent at the impact site.

ORIGINAL PAGE IS
OF POOR QUALITY

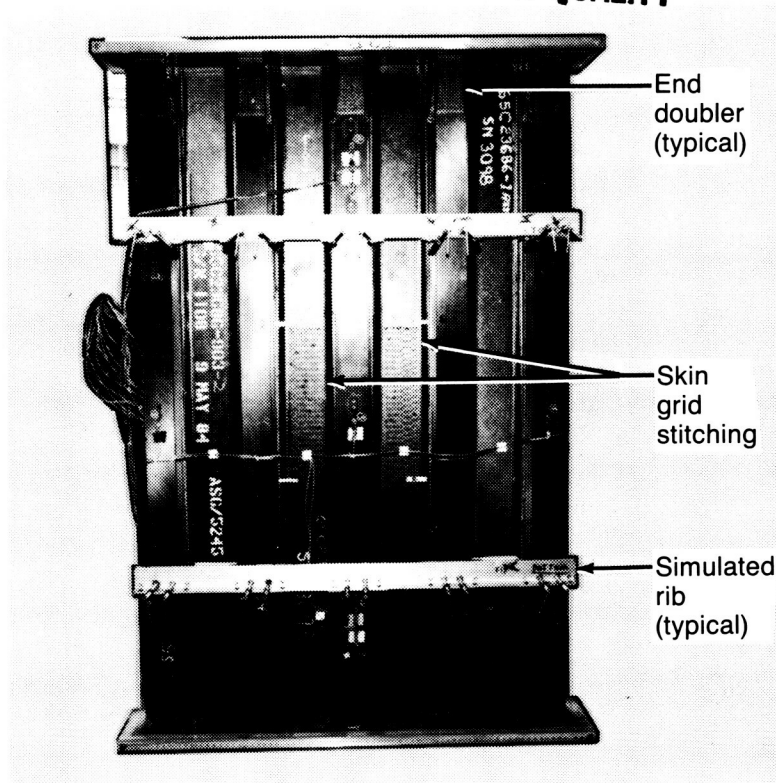


Figure 22. Five-Stiffener Test Panel

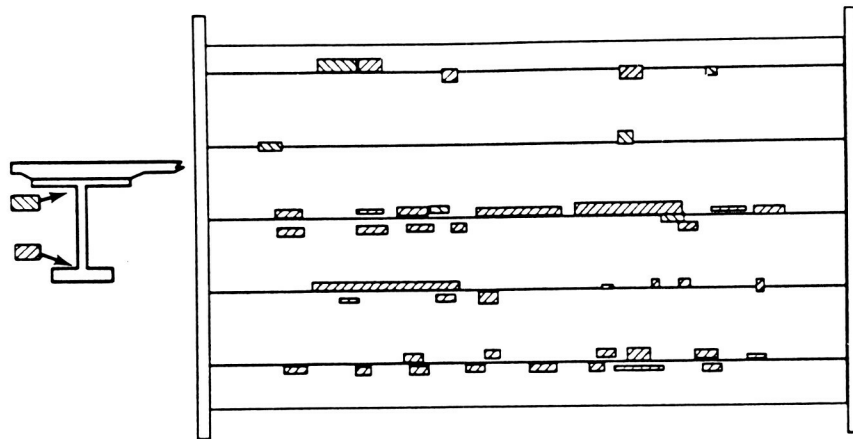


Figure 23. Pulse Echo Indications of Anomalies in Panel ①

ORIGINAL PAGE IS
OF POOR QUALITY

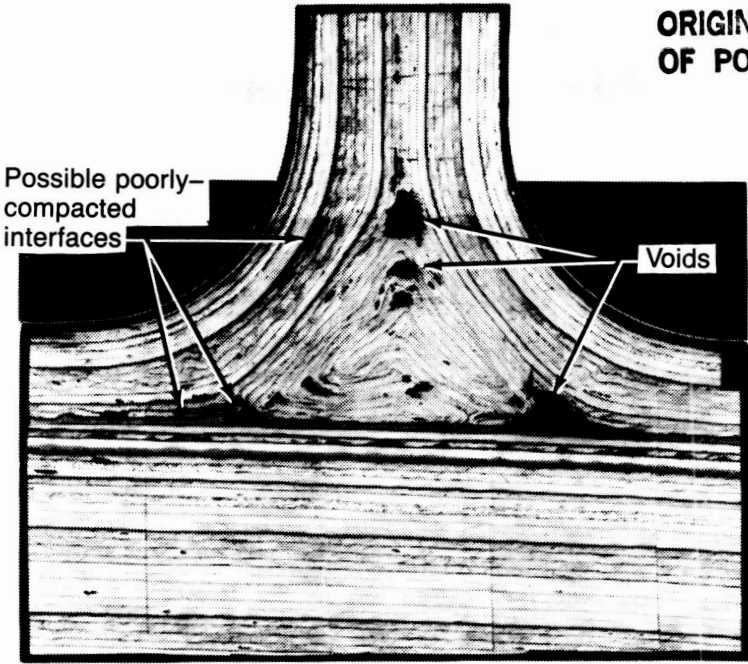
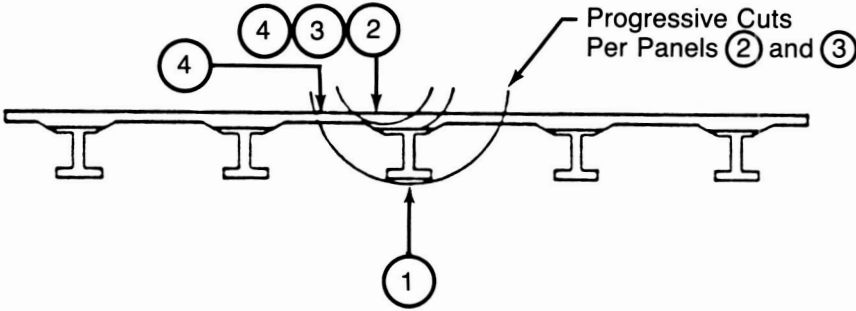


Figure 24. Photomicrograph of Sectioned Stiffener and Skin Area

Table 9. Large Panel Damage Tolerance Validation Test Program



Panel no.	Damage	Load case
①	400-in-lb impact on stiffener	Ultimate
②	2000-in-lb impact + progressive cuts through skin and stiffener	Limit
③		+ Continued safe flight
④	Multiple impacts on skin	Ultimate

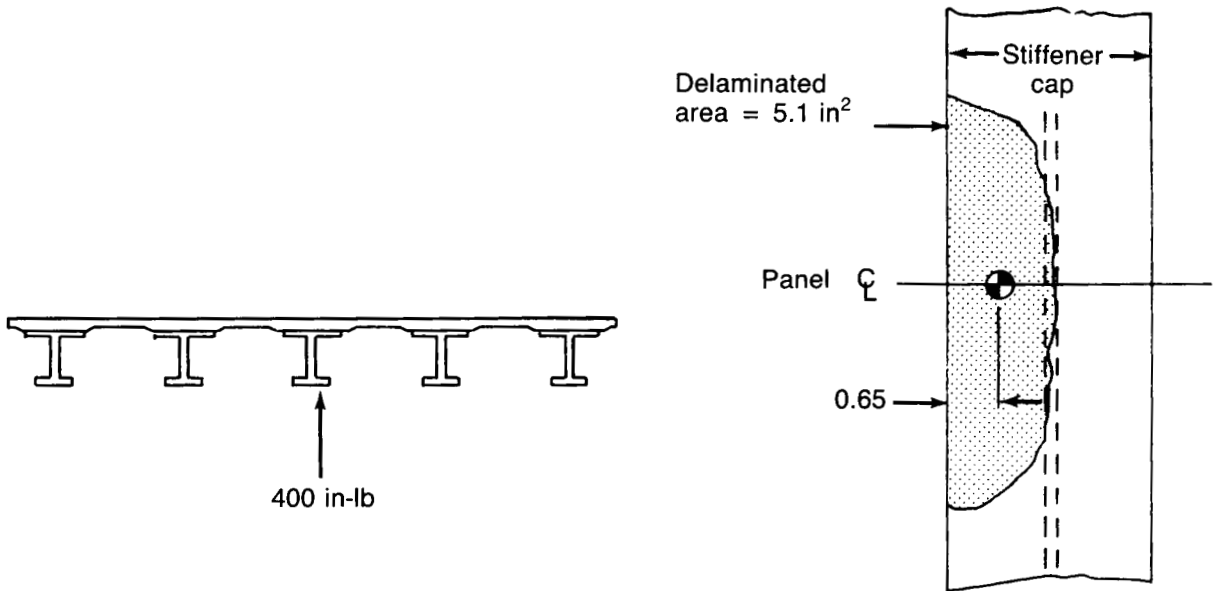


Figure 25. Stiffener Cap Damage to Panel ①

The 2000 in-lb impacts, with a 0.5-in diameter impactor, on the skins of panels ② and ③ produced visible surface damage. The dents were in excess of .07-in with some fiber breakage, and fiber break-out on the backside of the skin. Panel ②, which featured the skin-stiffener flange stitching, was found to have less total delaminated area than the non-flange-stitched panel ③.

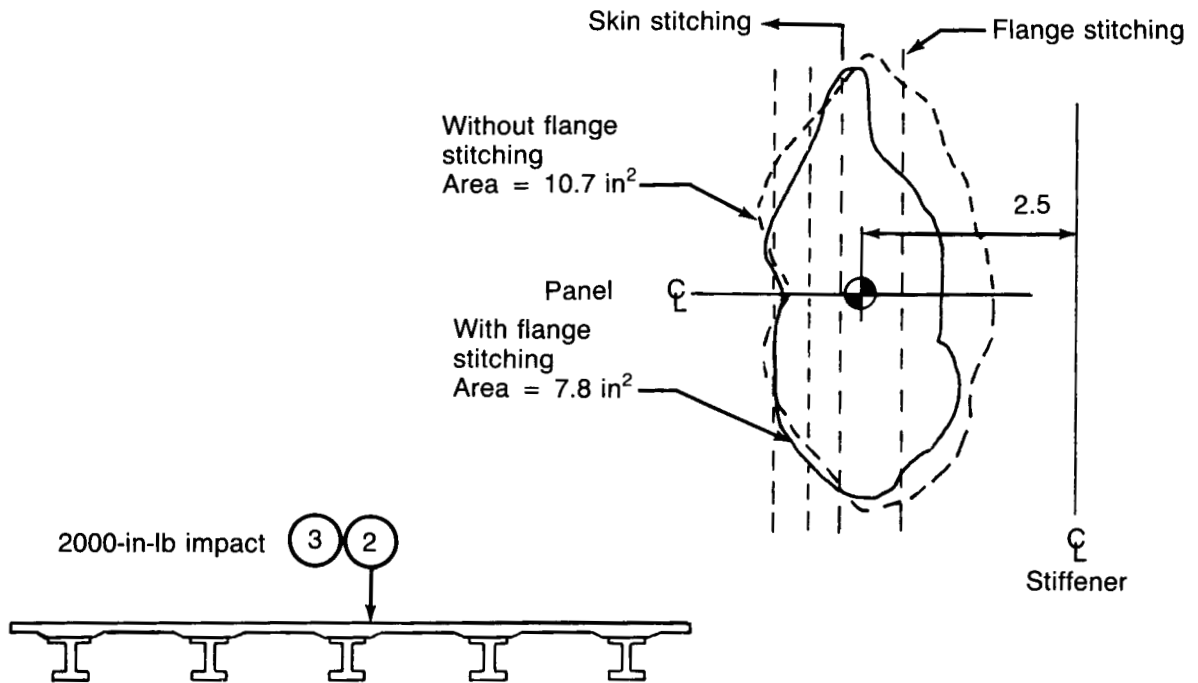


Figure 26. Inspection Results of Impacted Skins of Panels ② and ③

Panel ① failed at 755 kips (19.3 kips/inch end load) which is 97% of limit load. This load represents a P/AE strain of 0.004 and a gross area stress of 33.84 KSI. The panel was initially warped during fabrication with the panel bowing concave when viewed from the outside skin surface. Upon failure of the central stiffener through the impact site at 17.0 kips/inch end load, the skin immediately deflected in the opposite direction. The three center stiffeners separated from the skin over an area bounded by the aluminum ribs. The panel continued to carry load until overall panel failure occurred. At failure, the skin separated from all of the stiffeners, the stiffeners failed, and the load dropped to zero.

Panel ②, with the 2000 in-lb impact damage to the skin, was initially tested to the design limit load of 785 kips. Some delamination growth occurred (ref. fig. 27) due to this load which represents 20 kips/inch end load and a P/AE strain of .0041. The damage was increased incrementally by sawcut as shown in Figure 28. The panel was loaded to the continued safe flight load of 470 kips after each sawcut increment. There was no further evidence of growth due to these load cycles. After the third sawcut extension with the skin, central skin pad-up and stiffener flange completely severed with the 0.25-in wide sawcut for a length of 6.4 in, the panel was tested to determine the residual compression strength with this severe damage. The panel failed at a load of 573 kips which represents 122% of the continued safe flight load and a P/AE gross area strain of .0030. The failure, shown in Figure 29, was through the damage site with the skin and stiffeners fractured. There was no evidence of skin-stiffener separation except locally adjacent to the failure.

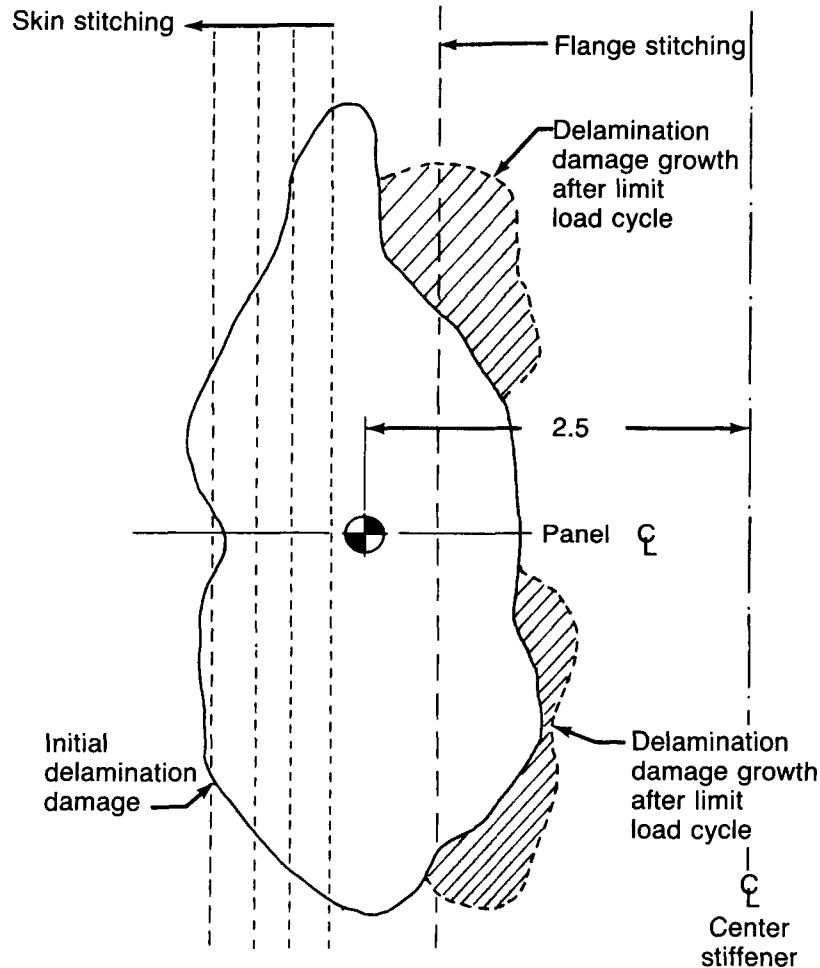


Figure 27. Pulse Echo Indications of Damage Growth After Limit Load Cycle of Panel ②

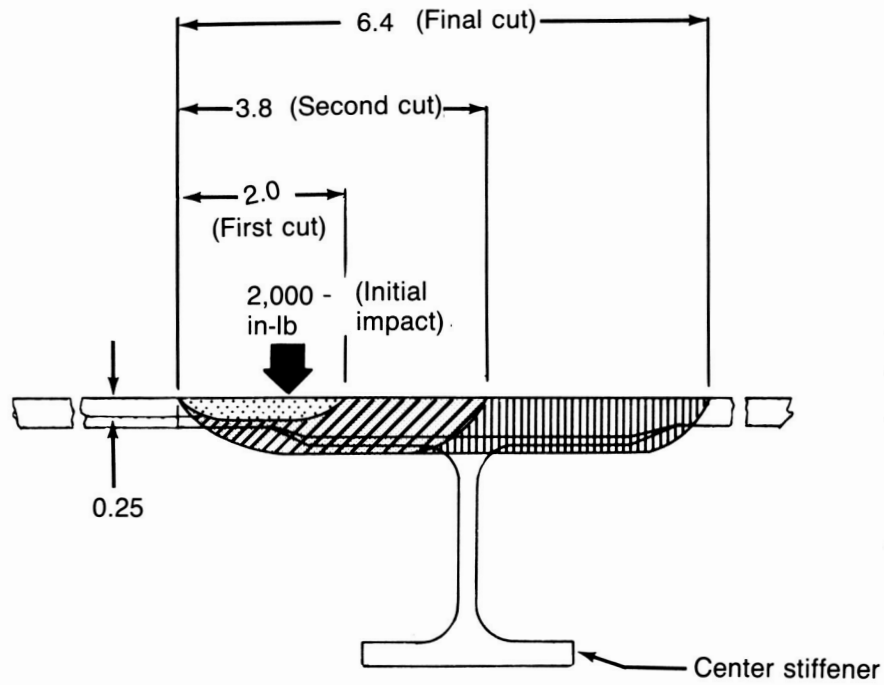


Figure 28. Sawcut Damage Increments of Panel ②

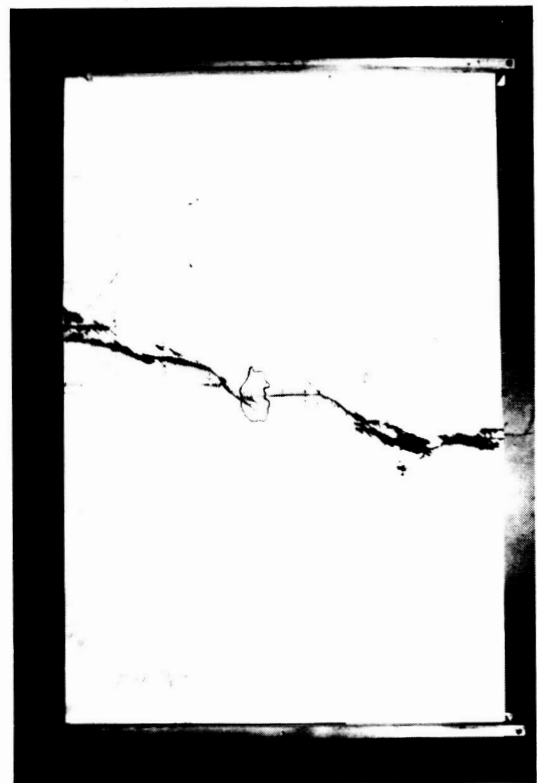
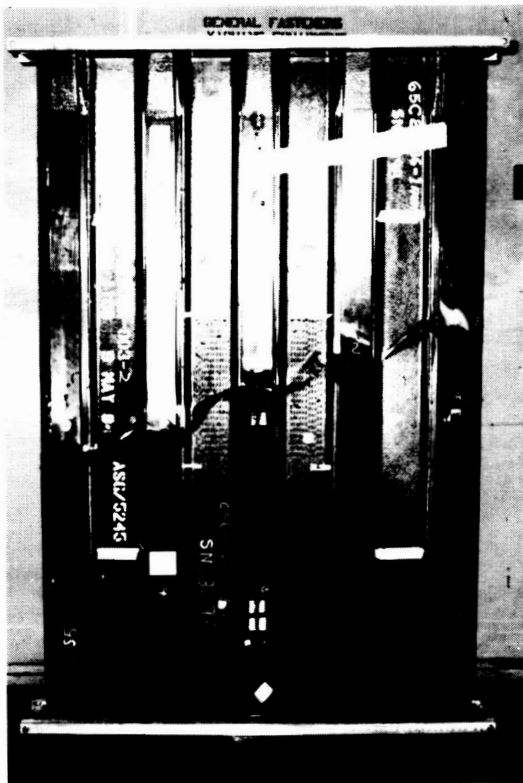


Figure 29. Failure of Panel ② After Sawcut Damage

ORIGINAL PAGE IS
OF POOR QUALITY

The loading sequence for panel ③ was similar to that of panel ②. The panel did not contain the skin-stiffener-flange stitching of panel ② and the area of delamination damage due to the initial impact of 2000 in-lb was larger than that of panel ②. The panel was initially tested to limit load and no damage growth was recorded due to this load cycle. The damage was then increased incrementally by sawcutting as shown in Figure 30.

The panel was loaded to the continued safe flight load after each sawcut increment. There was damage growth discovered after the safe flight load surveys of the third and fourth sawcut increments as shown in Figure 31. After the fifth sawcut extension with the center stiffener, skin pad-up, and skin completely severed for a total of 11.4 inches, the panel failed at a load of 460 kips. This load represented 98% of the continued safe flight load and a gross P/AE strain of 0.0024. The failure, similar to that of panel ②, was through the damage site with skins and stiffeners fractured.

Panel ④ was tested to the ultimate compression load condition with multiple impact damage. The panel was initially impacted with 1000 in-lb of energy, using the 1.0-in diameter steel impactor, on the skin at the edge of the pad-up ramp at site (A) as shown in Figure 32. The damage was barely visible with a dent of less than .04-in. The panel was loaded to the ultimate load of 1178 kips without failure. This load represents 52 KSI stress and a P/AE strain of 0.0062. The post-test pulse echo inspection indicated no damage growth.

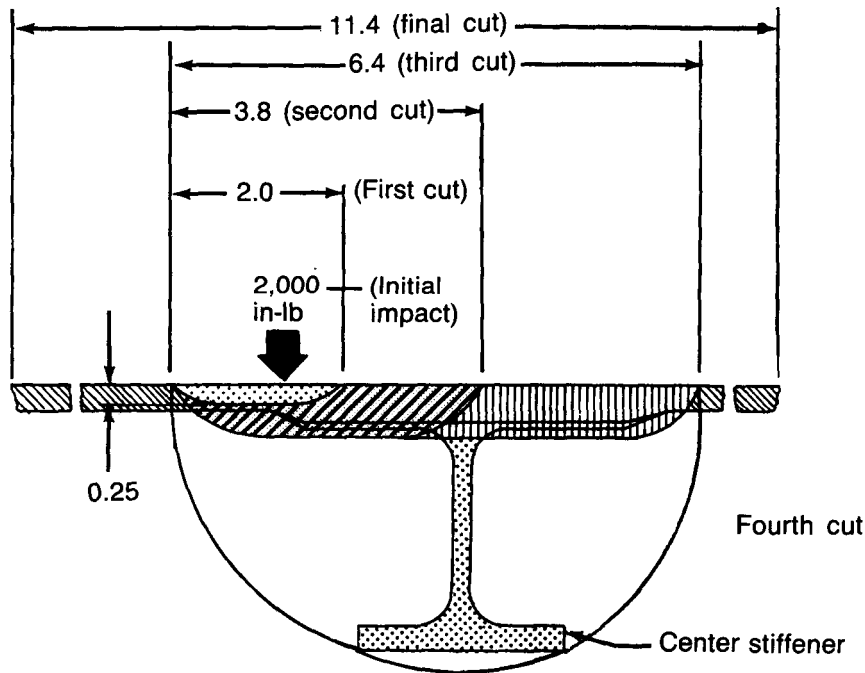


Figure 30. Sawcut Increments of Panel ③

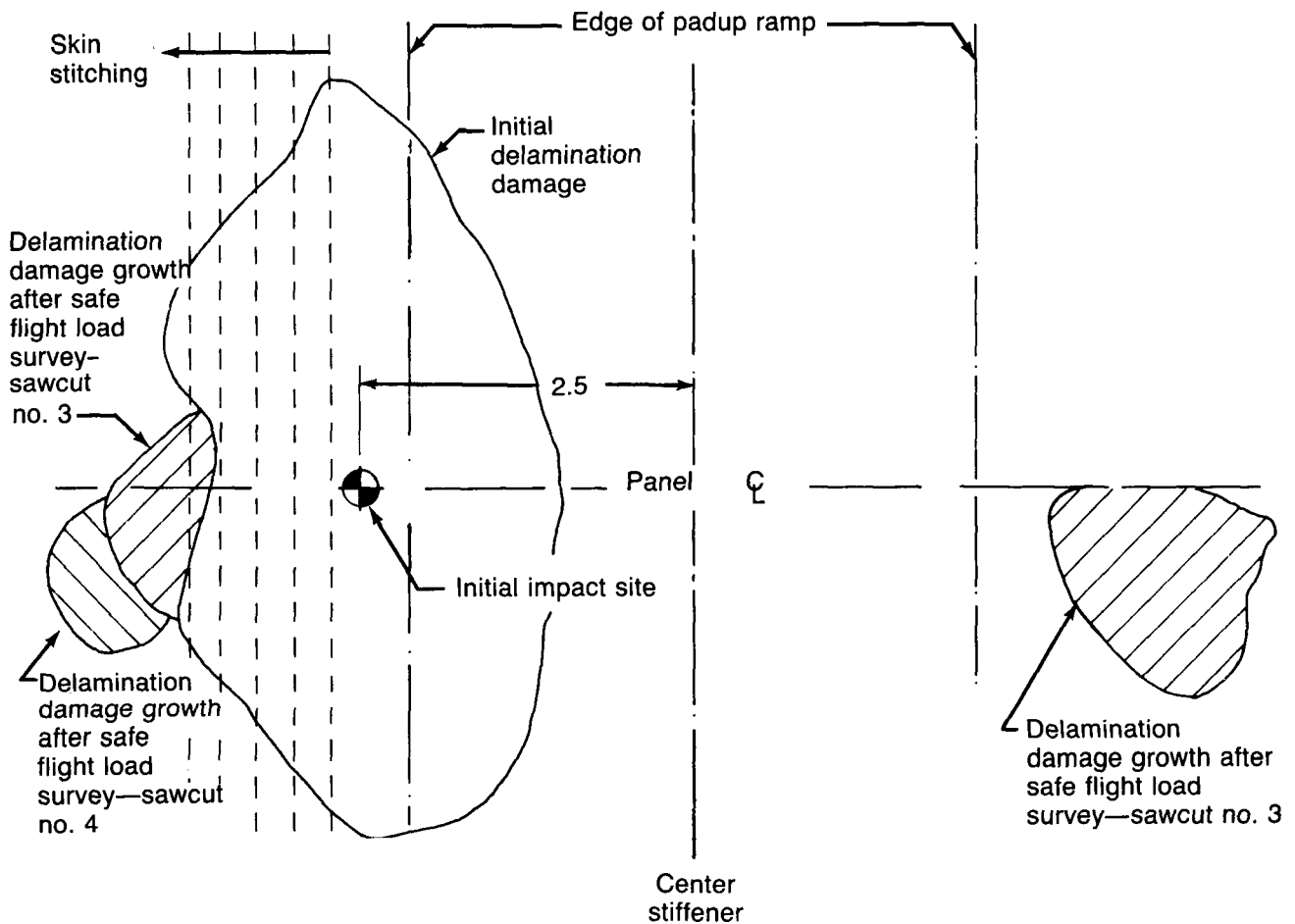


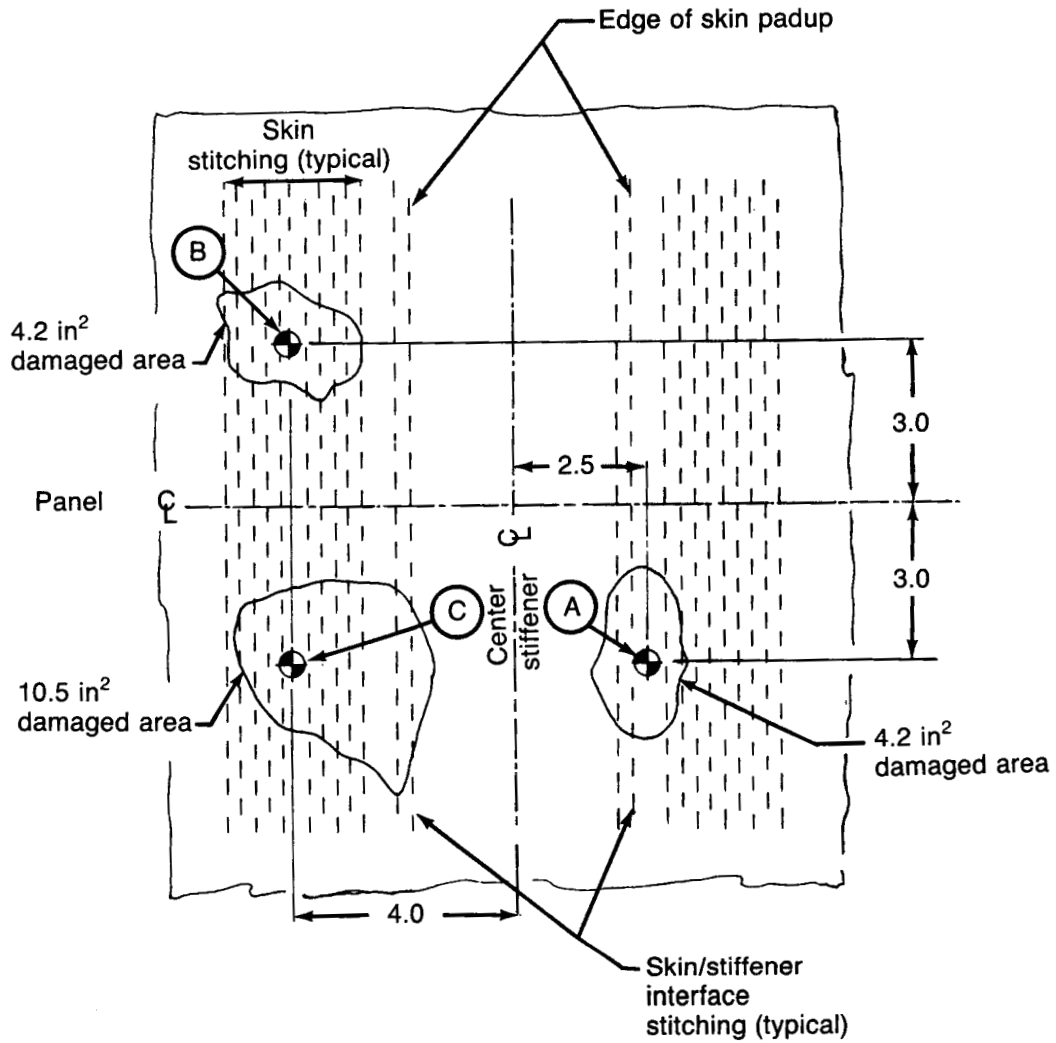
Figure 31. Pulse Echo Indications of Damage Growth in Panel ③

The panel was again impacted with 1000 in-lb of energy at site (B) on the skin between stiffeners. The damage was again barely visible with similar delaminated area indications to the impact at site (A). The panel was again loaded to ultimate load without failure. The post-test pulse echo inspection indicated no damage growth at either damage site.

The panel was finally impacted with 2000 in-lb of energy, using a 0.5-in diameter impactor, on the skin between stiffeners at site (C). The damage was easily visible with a dent similar in depth to those of panels (2) and (3) with some fiber breakage on the impact surface and fiber breakout on the inner skin surface. The panel was loaded to limit load of 782 kips without failure. This load represents a P/AE strain of 0.0041. The post-test pulse echo inspection did not detect any damage growth at any of the three impact sites.

The panel was finally loaded to failure to determine the residual compression strength. The panel failed through damage sites (A) and (C) at 1197 kips. This represents 102% of the design ultimate load and a P/AE strain of 0.0063. Figure 33 presents the failed panel with the failure running through the 2000 in-lb damage site.

The four panel tests of the large panel damage toleration validation program addressed all of the load cases and damage conditions of Table 3. The load goal of each condition was successfully attained with the exception of the stiffener damage case of panel ① .



- Ⓐ 1000 in-lb (1-in-dia impactor) on skin at edge of ramp
- Ⓑ 1000 in-lb (1-in-dia impactor) on skin between stiffeners
- Ⓒ 2000 in-lb (0.5-in dia impactor) on skin between stiffeners

Figure 32. Impact Sites and Pulse Echo Inspection Results of Panel ④

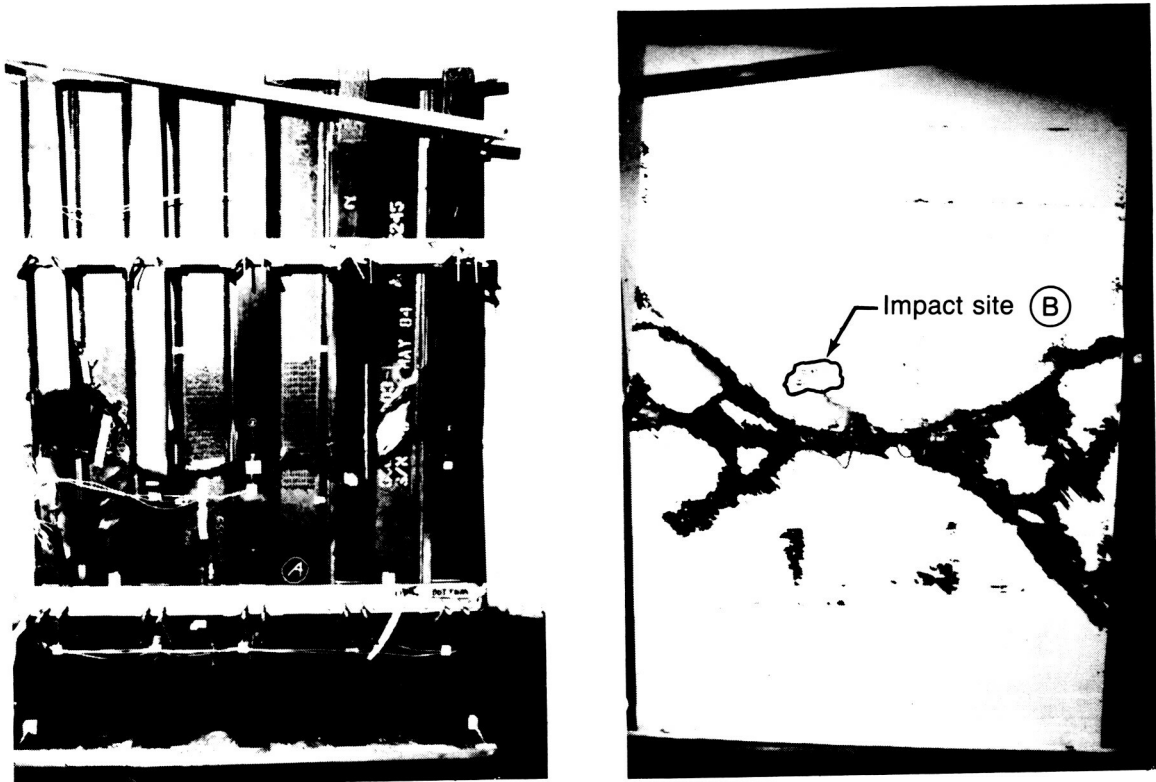


Figure 33. Failure of Panel (4) After Multiple Impact Skin Damage

The results of the five-stiffener test program are presented in Table 10.

Table 10. Five-Stiffener Panel Test Results

Panel no.	Damage	Load Case	Failure end load (kips/in)	Failure stress (ksi)	Failure strain, P/AE (in/in)	Skin/stiffener flange interface	
						Stitched	Nonstitched
1	400-in-lb impact on center stiffener cap with 1.0-in-dia impactor	Ultimate (30 kips/in)	19.31	33.84	0.004	X	
2	6.4-in sawcut through skin, center skin padup and stiffener flanges	Continued safe flight (12.0 kips/in)	14.60	25.5	0.003	X	
3	11.4-in sawcut through skin, center skin padup and center stiffener	Continued safe flight (12.0 kips/in)	11.77	20.65	0.0024		X
4	(a) Multiple skin impacts with 1.0-in-dia steel impactor: 1000 in-lb at edge of ramp, 1000 in-lb between stiffeners (b) 2000 in-lb on skin between stiffeners with 1/2-in dia. impactor	Limit (20 kips/in)	30.60	53.6	0.00633	X	

WING PANEL REPAIR DEMONSTRATION

The large panel damage tolerance test program demonstrated the capability of the final panel design to meet the wing panel design criteria. The program assessed the effect of skin and stiffener damage on the ultimate, limit, and continued safe flight load capabilities of the final upper surface wing panel design. One aspect of wing panel design that had not been evaluated was repair of major damage to restore ultimate load capability.

A five-stiffener panel of the same configuration as used in the large panel damage tolerance validation test program was damaged with a sawcut. The sawcut severed the center stiffener, skin pad-up and skin for a total length of 8.0 in. The basic repair philosophy was to use a typical service repair that requires no special equipment. The repair was made using steel plates and channels assembled to the panel with steel bolts. Figure 34 presents a cross-section through the repair. The repair design

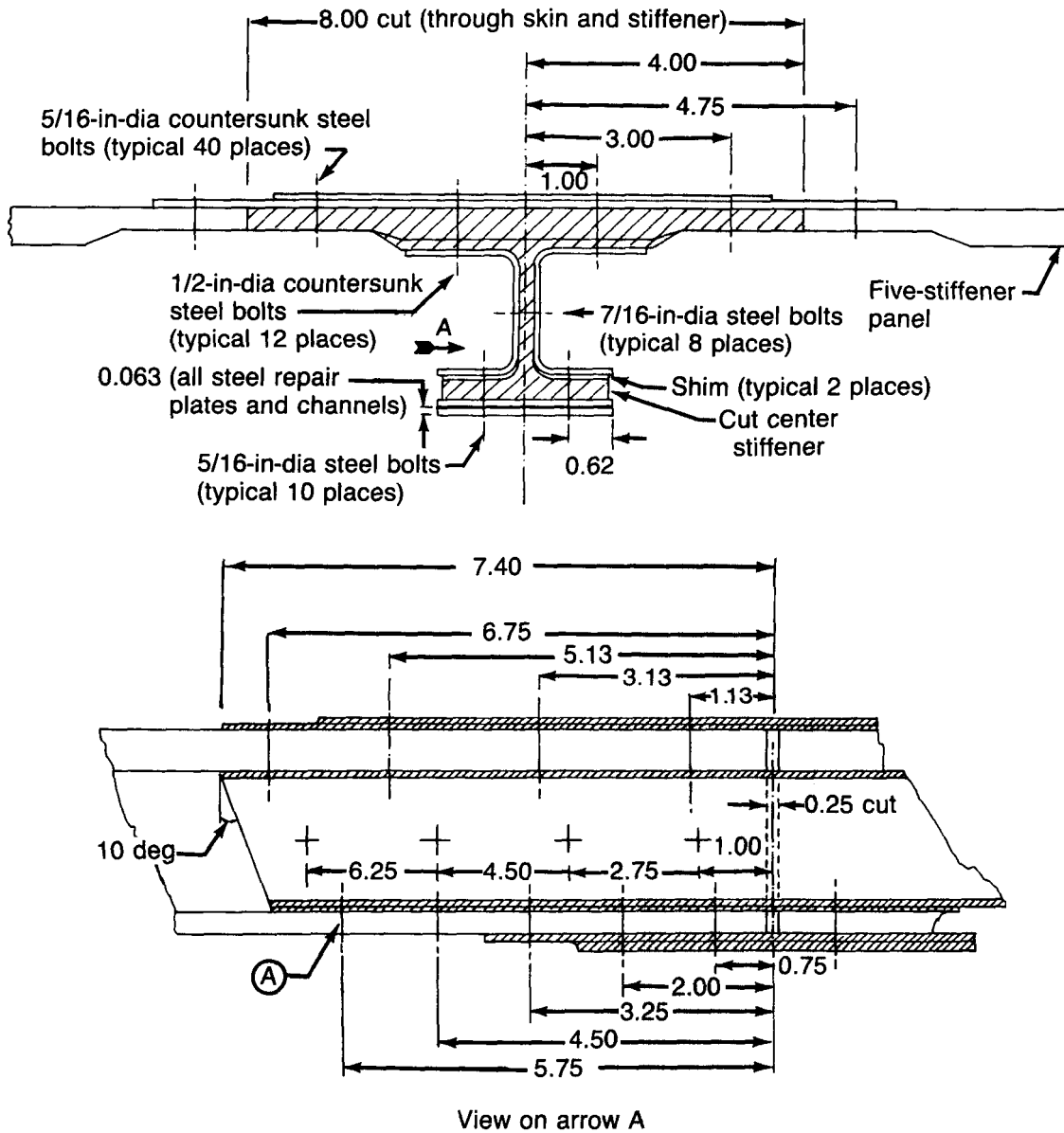


Figure 34. Initial Repair Configuration

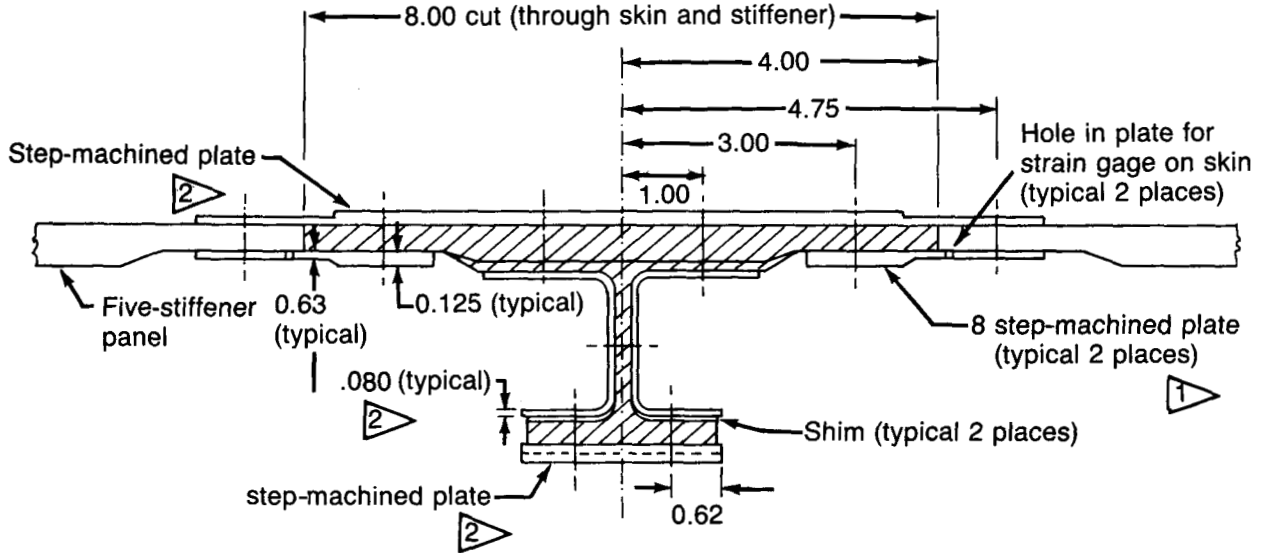
matched proportional element stiffnesses (AE) while replacing the cut AE with 125% of that lost. Bending strains were kept to a minimum by tailoring the load paths, and where possible, the fasteners were sized to develop the repair element capabilities. The steel plates and channels were all fabricated from 0.063-in 4130 steel sheet heat treated to 180 ksi ultimate tension strength. The fasteners were 180 ksi steel Hi-Loks installed wet with fuel tank sealant in close tolerance holes. The fasteners in the skin repair had countersunk heads typical of wing panel structure.

The test configuration and instrumentation was similar to that of the large panel validation tests (ref. fig. 18) with the exception of the Moire fringe which was deleted. Additional strain gages were added to monitor the strains in the steel repair hardware, and the strain in the skin at the sawcut tip.

The panel was loaded incrementally to 600 kips twice before the test was terminated due to poor strain distribution from the strain gages on the repair plates and high strain in the skin at the tip of the sawcut.

A post-test analysis of the results indicated that the skin repair countersunk fastener heads were probably not sealed well enough to effect consistent load transfer. The countersunk fastener sizes used resulted in a "knife-edge" condition in the outer skin repair plate. It was decided to replace these fasteners with shear type protruding head bolts to alleviate this problem. It was also determined that the skin repair should be a double-shear configuration with a repair plate on the inside skin surface in order to reduce the strain at the tip of the sawcut in the skin.

The above modifications were made to the repair. Also, the stacked 0.063-in steel plates replaced with stepped machined plates with the gage of the steel channels increased from 0.063-in to .080-in to minimize load line shift due to the increase in skin repair plate AE. Figures 35 and 36 present the modified repair configuration.



Note:

- 1 Additional repair hardware
- 2 Modified repair hardware
- All fastener protruding head oversized up to 1/32 in from original repair

Figure 35. Modified Repair

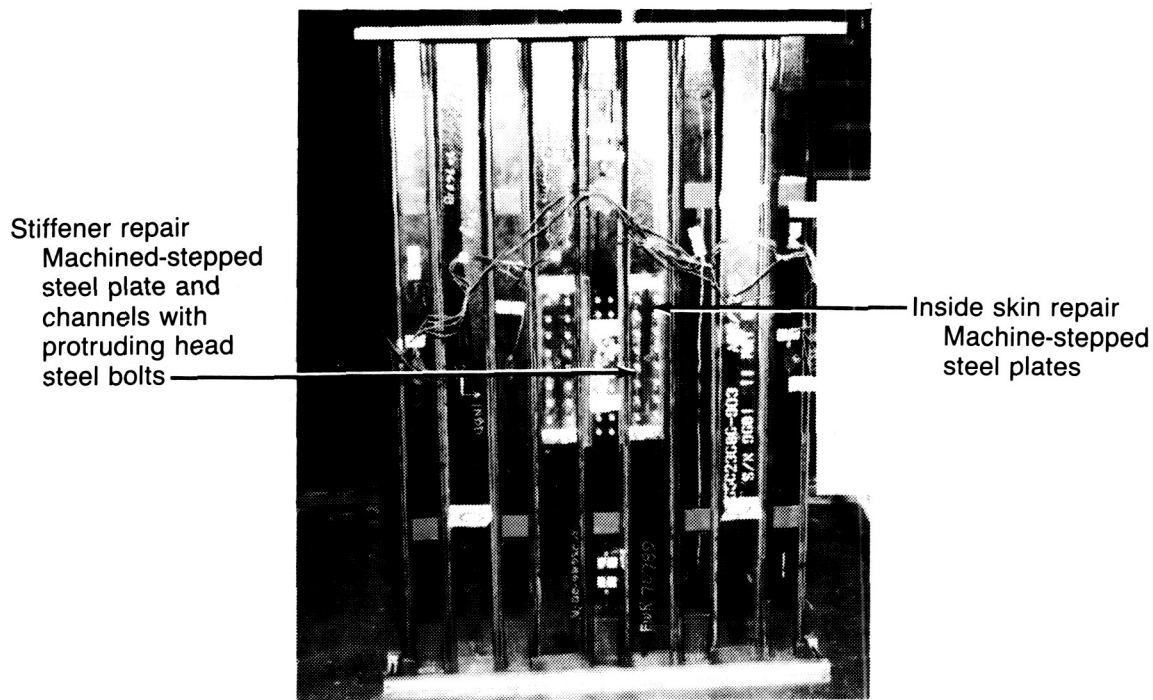
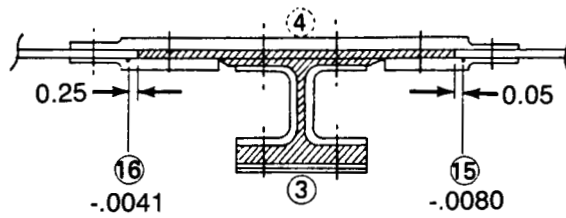
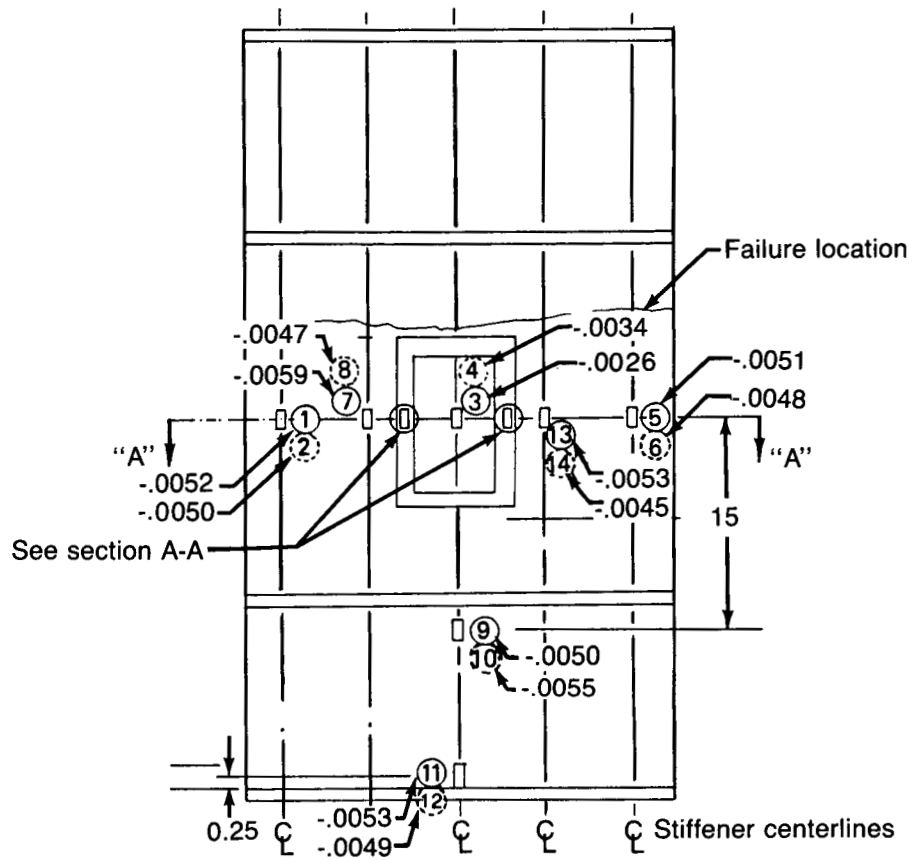


Figure 36. Modified Repair Panel

One additional change was made to reduce the tolerance between the fasteners and the fastener holes to obtain more consistent load transfer. The holes were reamed to size so the oversize fasteners were almost a net fit and the fasteners were matched to the holes. Some fasteners, particularly at the skin pad-up and stiffener flanges, had to be installed by cooling them in liquid nitrogen to reduce the shank diameter during installation. After the panel had been reinstrumented, the outside skin repair was faired-in with aerodynamic "Bondo" to smooth out the effect of the plates and protruding head fasteners.

The panel was again loaded incrementally to 600 kips at which the strain output was scrutinized for load distribution and compared to the strain output of the original test. The strain distribution was considerably better than that of the previous loading with good load distribution into the steel repair plates. The loading was continued and at about 800 kips the acoustic emissions indicated damage occurring (or growing). Total panel failure occurred at 996 kips. This load represents 84% of design ultimate load and a P/AE strain of 0.0052.

The failure originated at the first fastener in the stiffener cap repair (ref. point A in fig. 34) and propagated across the panel outside of the repair plates. All five stiffeners failed and were separated from the skin in a manner similar to that of the five-stiffener panel with the center stiffener cap impact damage. The strain in the skin, .05-in from the end of the sawcut, was .008 at failure. There was no evidence of damage emanating from either end of the sawcut. The failure location and strain values are presented in Figure 37. Figure 38 shows the panel at failure with the skin separated intact from the stiffeners.



Section "A-A" — through repair

Figure 37. Repair Panel Failure Location and Strains

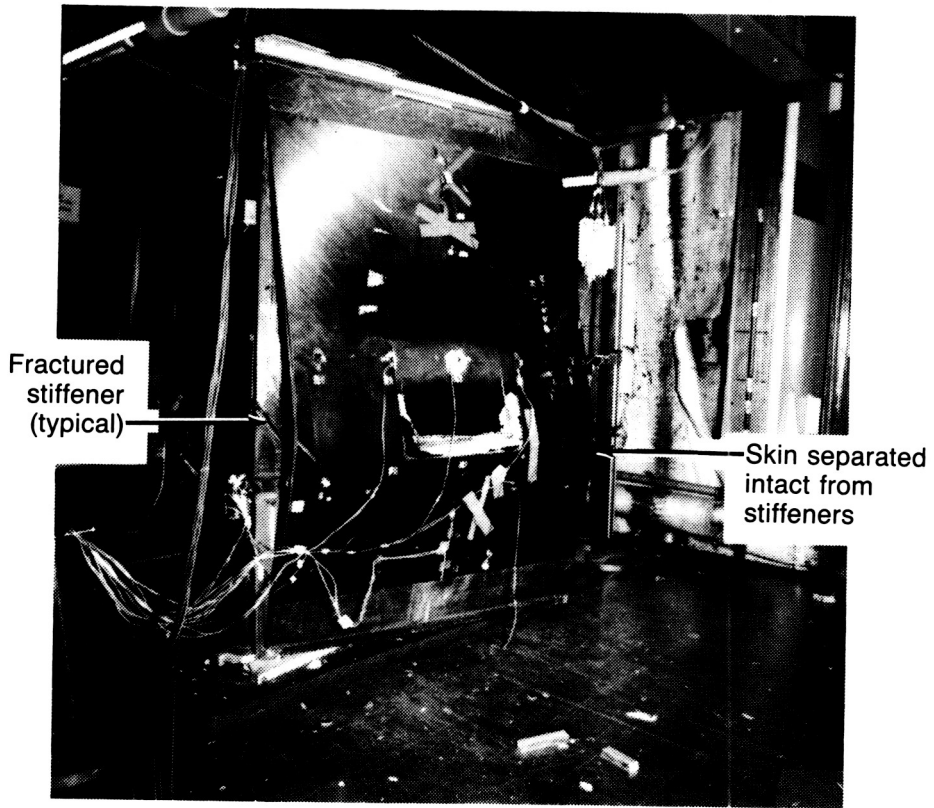


Figure 38. Repair Panel Failure

PANEL TEST SUMMARY

Figure 39 summarizes the results of the Phase I and Phase II panel tests. All of the panel test data for both Phase I and Phase II are shown relative to the design strains and corresponding stresses. The stresses were normalized for full skin bays, assuming the skins were fully effective. This assumption was validated by the strain gage data which in all cases indicated no skin buckling prior to failure. The strains are gross area P/AE strains using moduli gained from basic material property coupon tests.

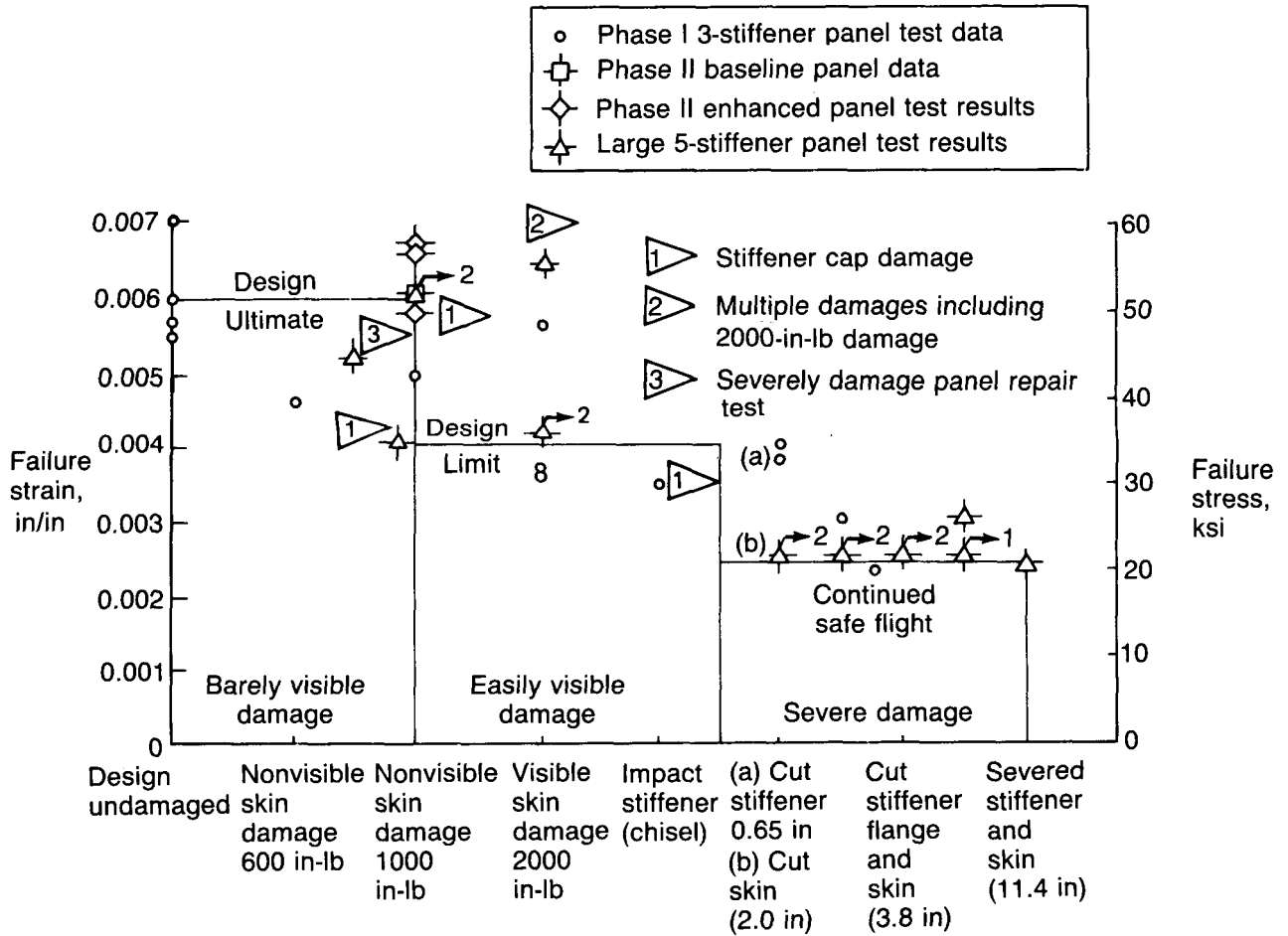


Figure 39. Damage Tolerance Validation Test Results

**ORIGINAL PAGE IS
OF POOR QUALITY**

CONCLUSIONS

The LCPAS program has shown systematic progress toward the overall program goal of improving composite wing design capability. This goal was to achieve 0.006 design strain for both tension and compression loaded wing panels. This has been successfully demonstrated on the critical compression-loaded upper surface panels with service damage. In all of the design load cases (ultimate, limit, and continued safe flight), the final damage tolerant design demonstrated adequate capability for typical service damage.

The wing structure damage assessment identified delaminations caused by impact events to be the critical form of damage for compression loaded graphite composite wing panels. The study identified four approaches to reduce the effects of damage: (1) develop tolerant structure, (2) improve quality control practices in both manufacturing and service, (3) improve NDE methods for detecting damage during manufacturing, and (4) develop service inspection techniques to ensure that critical service damage is identified.

The results of the material screening tests indicated that the thermoplastic AS4/PEEK was significantly tougher than the thermoset materials tested. The AS6/5245C was found to be the toughest of the thermosets tested and was chosen for the five-stiffener validation test panels.

The results of the damage growth coupon tests and the three-stiffener baseline panel tests showed that constant amplitude compression-compression ($R=10$) fatigue cycling is more harmful to impact damaged specimens and panels than the spectrum load cycling typical for commercial airplane upper wing surface panels. It was also found that to grow damage in impact damaged three-stiffener panels, the maximum cyclic loads had to be in excess of 60% of the ultimate design load.

The damage growth coupon tests also demonstrated that through-stitching of laminates reduces delamination damage from impact and improves residual compression-after-impact strengths. This feature, when used in conjunction with other damage tolerance design features of the enhanced design, also improved the residual compression strength of three-stiffener panels.

The program has highlighted the need to address barely visible stiffener cap damage which is possible in the manufacturing environment. Quality control procedures will need to be evaluated to prevent this damage.

The repair panel test demonstrated the repairability of the final design. The repaired panel achieved 84% of design ultimate load before failure occurred at a single shear fastener detail in the stiffener cap. The repair test showed that single shear load transfer and countersunk fasteners are not good design details for heavily loaded composite repairs. This program has demonstrated that with good design details and care in repair, economical service repairs for primary wing structure designed to .006 strain can be achieved.

REFERENCES

1. McCarty, J. E.; and Roeseler, W. G.: "Durability and Damage Tolerance of Large Composite Primary Aircraft Structure (LCPAS)." NASA CR-3767, January 1984.
2. "ACEE Composites Project Office (Compiler), Standard Tests for Toughened Resin Composites Revised Edition." NASA RP-1092, July 1983. (Supercedes NASA RP-1092, 1982.)
3. Wang, A.S.D.; Kishore, N. N.; and Feng, W. W.: "On Mixed Mode Fracture in Off-Axis Unidirectional Graphite-Epoxy Composites." Progress in Science and Engineering of Composites, Volume 1 (1982).
4. Byers, Bruce A.; "Behavior of Damaged Graphite/Epoxy Laminates Under Compression Loading." NASA CR-159293, August 1980.

APPENDIX
WING STRUCTURE DAMAGE ASSESSMENT

M. N. Gibbins, P. J. Smith, R. D. Wilson
Boeing Commercial Airplane Company

SUMMARY

In aircraft structures, damage is an unintended event causing degraded structural performance. Damage may be visible or hidden, and may appear in critical or noncritical locations. Damage may occur during manufacturing in the form of flaws, voids, gouges, and impacts or during airplane service in the form of impacts and gouges. It is important to consider damage when designing composite structures because damage reduces strength, particularly compression strength.

Boeing has identified four approaches to reducing the negative effects of damage: (1) develop damage tolerant structure designs, (2) improve quality control to reduce critical manufacturing and fabrication damage, (3) improve non-destructive evaluation (NDE) methods for detecting damage during manufacturing, and (4) develop in-service inspection techniques ensuring that critical damage is identified.

MANUFACTURING DAMAGE

As with aluminum structure, composite aircraft structure is susceptible to damage from a variety of sources during manufacture and service. The critical forms of damage in composites are substantially different from critical damage in aluminum due to differences in material structure, fabrication techniques and damage growth mechanisms.

Fabrication processes provide the opportunity for the introduction of several damage/defect types, although some may not have a critical effect on strength. Some of the more common and critical defects are considered below.

Panel Waviness, Warpage, Contour Deviation—These defects (Figure 1) are usually caused by warped tools or thermal expansion mismatch between the part and the tooling, and primarily affect assembly and aerodynamic requirements.

Physical measurement of the parts is the current inspection method. Typical tolerance limits are .005 in/in and .030-in maximum in any direction. Use of thermally stable or matched tooling may correct the problem.

Laps, Gaps, Crossovers—These defects (Figure 2) are caused by poor manual layup methods and automatic ply layup and are nearly impossible to detect without a cross-sectional view of the laminate. Current tolerances allow a 0.1-in maximum overlap or gap. Some testing indicates that these defects can cause approximately a 10% strength reduction.

Foreign Body Inclusions—Prevention of inclusions requires inspection scrutiny during layup and contaminate free layup areas. Inspection for inclusions can be performed with through transmission ultrasonics (TTU), ultrasonic pulse-echo, or x-ray, although small inclusions will be difficult to identify. Inclusions can reduce interlaminar strength and cause local stress concentrations.

Porosity—Low pressure or loss of pressure during cure, or layup moisture ingestion prior to cure can cause porosity. Successful non-destructive porosity identification can be made with x-ray radiography and with ultrasonics if done carefully and with sufficient prior calibration of the electronics.

Severe porosity (greater than 1% by volume) can reduce interlaminar and compression strength, as shown in Figure 3, although strength loss may not occur for Boeing's current porosity tolerance limit of 0.5%. It should be noted that obtaining consistent porosity measurements is difficult and results may depend on the technique used. Figure 3 also shows that in terms of strength, a .25-in diameter hole will overshadow porosity above the tolerance limit.

Delaminations—This is one of the most critical forms of damage in laminated composite materials. There is a high probability of finding delamination with ultrasonics (TTU, Pulse-Echo) provided the defect is of sufficient size (usually the tolerance is one half inch diameter). The criticality of the delamination depends on the location and the size (area or length).

Delaminations can be caused by poor bonding or curing, impact damage, and poor trimming operations, and can be minimized by tool design, improved handling practices, and good structural design practices.

Impact During Fabrication and Assembly—Dropped tools are a risk and can cause a wide range of impact energy intensity. For example, a wrench dropped from three ft may inflict only 70 in-lbs, while a drill motor dropped from 40-ft could inflict 3800 in-lbs of energy to a surface.

INSERVICE WING DAMAGE

During routine operation of commercial airplanes, events occur that represent a damage threat to composite wing structures. Events most frequently reported in incident or damage reports supplied by airplane operators from 1970 through 1982 are discussed below. All events involved aluminum structure.

Engine Cowling Separation—Engine cowling parts have contacted wing surfaces and caused scratches or gouges. This primarily occurs on the lower wing surface.

Tire Blowout—This event occurs only on the ground during the take-off roll or during landing. There have been reports of tire or wheel particles causing scratches or punctures, usually in the lower surface.

Engine Disintegration—This event is one of the highest energy threats. The event involves the engine shedding one or more fan, turbine, or compressor blades. Wing damage ranges from scratches in the lower surface to penetration of both lower and upper surfaces with stiffener, rib, and spar damage also possible.

Less Frequently Reported Events—One incident report described an over-wing scaffolding causing scratches and gouges in the upper surface. Another report described the discovery of a bullet hole in the vertical fin of a 737. In this case, the skin and one rib was damaged. The slug was found inside the fin, and was identified as a 38-cal. pistol round.

Specific Damage Descriptions—(1) A typical abraded area in a 747 lower wing surface had scratches .010-in deep and was about 3-in in diameter. (2) A gouge was recorded as 5-in long, 1/8-in wide and .06-in deep. (3) Wing skin punctures were up to 4-in long.

Dents in the wing skins are another form of damage which have been reported. Dents within a specified tolerance are allowed, and a typical repair method is to fill in and smooth the depression. The impacts which cause dents and depressions in aluminum may affect composite structures in substantially different ways. Impact energy levels were not estimated for any of the events.

A non-mechanical form of damage could occur from a fire or lightning strike. Several reports of wheel and engine fires were associated with the mechanical damage events described above. Lightning strikes pose hazards to composite aircraft structure to which aluminum structure is less vulnerable. A lightning strike on a NASA ACEE composite 727 elevator caused damage 1½ by 3 in to the graphite/epoxy trim tab.

Hail and Ice Balls—Airlines have reported few incidents of hail damage; however, hail does pose a damage threat to thin structures. After a severe hail storm in Fort Worth, Texas, investigators of the resulting damage of airplanes on the ground estimated the inflicted energies up to 360 in-lb.

IMPACT DAMAGE ON WING SKINS

Past studies (References 1 and 2) have shown that impact damage can be more detrimental to compression strength than either an open hole or simulated delaminations. Research has shown that impact damage has greater influence on compression strength than on tension strength. Recent coupon and panel residual strength test data reveal that impact damage is the critical form of damage in exposed airplane structure and over-shadows other forms of damage. This is because impact damage consists largely of delamination which is the most serious form of damage in composite wing panels due to the presence of compression loading on both upper and lower surfaces.

The general impact energy criteria Boeing uses for composite structure is that energy level which produces a barely visible indication on the surface. Barely visible is the minimum damage that is likely to be discovered during inspection. The impact energy standard currently used by Boeing for the upper wing surface is 1000 in-lb using a 1.0-in diameter spherical impactor.

This standard encompasses possible fabrication, assembly, and maintenance impact events. A single impact of 1000 in-lb is considered representative of a worst case event, and more probable than extremely remote (1:10⁹).

An alternate impact criteria was developed in the Air Force contract "Damage Tolerance of Composites," and involves a variety of damage events assumed to be present in the structure due to the manufacturing and assembly process. In addition, criteria are defined for the damage assumed to occur at the most adverse time during the aircraft's lifetime. These damage cases included misinstalled fasteners, scratches, delamination, dents, through penetration, and specific impact events.

CRITICAL LOCATIONS OF WING IMPACT DAMAGE

Because compression members are more sensitive to damage, the locations to be considered here are primarily the wing upper surface. The general exterior areas of the wing differentiated for impact criticality (fig. 4) are as follows:

- **On skin between the stiffeners**—On current wing skin designs at least 50% of the panel area is between stiffeners. Due to the low flexure stiffness, this area will experience more delamination than the area over the stiffeners for a given impact energy level.
- **On skin at the stiffeners**—Testing has demonstrated that this is a less critical area than between the stiffeners since damage indications are visible at lower energies and the resulting delaminations are less extensive.
- **On skin at stiffener pad-up ramp**—Recent tests have indicated that impacts at the skin edge of the pad-up ramp may be one of the most critical locations.
- **Stiffener cap**—Damage to a stiffener cap must be considered because it carries a substantial portion of the stiffener load. Recent tests have shown that a barely visible stiffener cap impact damage of 400 in-lb can significantly reduce the residual compression strength of stiffened panels. This form of damage may occur during manufacturing and assembly.
- **Edges and corners of a panel**—Impacts at these locations are likely to produce more severe damage because the area lacks surrounding structure and is less constrained.
- **Ribs and Spars**—Impacts on the skin near the ribs and spars are considered less severe because they provide the panel with support against flexure in much the same way as the stringers. Fasteners, if used as the attachment method, will provide additional constraint against delamination.

SERVICE MAINTENANCE AND INSPECTION METHODS

SERVICE MAINTENANCE PRACTICES

Service experience with commercial airplane wing skins is limited to aluminum structure. Experience is being acquired with composite secondary structure such as spoilers, ailerons, flaps, and elevators, on Boeing 757 and 767 airplanes. Graphite-epoxy spoilers have been in service on 737 airplanes since 1973 under NASA contract NAS1-11668. Primary structure in the form of a Boeing 737 stabilizer has been flight tested and FAA certified, and several are scheduled to enter service in 1984. In addition, the Boeing 737-300, scheduled to enter service in November 1984, uses graphite epoxy on all control surfaces, including spoilers.

Composite components such as these are routinely repaired if damaged. Repair usually involves cutting away the damaged composite skin and core material. Replacement prepreg and core are cured in place under a partial vacuum bag and heat blankets at temperatures up to 350°F. The higher temperatures are used for more strength critical areas. Scratches, gouges, and holes in aluminum wing skins are routinely repaired. The goal at Boeing is to develop composite wing skin designs which can be repaired with an economic impact not greater than for current metal repair practices.

SERVICE INSPECTION SCHEDULES

Commercial inspection practices for aluminum wing structure are outlined in Table I. The inspection intervals shown are based on average fleet utilization and service data.

Preflight and transit inspections include scrutiny of the wing lower surfaces, wing tips, flaps, slats, ailerons, static dischargers, lights, and fuel tank sumps. Wing upper surfaces are not routinely checked under this category.

Table 1. Average Reported Fleet Service Inspection Intervals

	Service interval	Time spent on wing skin (hrs)	Likely inspection methods
Transit	Each flight	0.1 	} Visual
Preflight	Daily	0.4 	
A check	80 flights	0.4	
B check	370 flights	0.4	} Visual, ultrasonic, eddy-current, X-ray
C check	1,300 flights	4.0	
Structural check (or D check)	13,000 flights	140 	

 Only lower wing skins checked

 Includes time required to remove access panels and doors

The "A" and "B" checks include all the preflight and transit wing check items. In addition, the "B" check includes visual checks of the flap actuators. The "C" check includes extensive inspection of the upper and lower surfaces, flight controls, skin joints, access panels, and spars. The structural or "D" check requires extensive inspection of interior and exterior wing upper and lower surfaces including stiffeners. For economic and efficiency considerations, airlines have been recently replacing B checks with multiple A checks and replacing D checks with multiple C checks. For example, a 3C check item would be inspected during every third C check time period. A 2A check item would be inspected during every second A check time period. All critical structural items continue to receive appropriate attention.

As composite materials are introduced into commercial airplane primary structure, inspection practices will need to be reviewed. For instance, the strength reduction of compression members due to impact damage will require more frequent inspections of the wing upper surfaces. Specifications for composite structure inspection will require concurrence by the airlines; therefore, airline representatives must be consulted during drafting inspection procedures. Airlines need to ensure inspection requirements are flexible enough to fit into current scheduling practices. Inspection procedures for composite structure must be compatible with current practice and must not disrupt servicing of the established aluminum structure fleet.

INSPECTION METHODS

The unique nature of composite materials will require the development of new inspection methods. Several methods described below are in current use; others have development potential.

Through Transmission Ultrasonics—The primary non-destructive evaluation (NDE) method used on large graphite/epoxy structural components to identify delaminations and disbonds is through transmission ultrasonics (TTU). One hundred% of the 757 and 767 control surface and nacelle panels are inspected in this way. Coupling between the part surfaces and the transducers is usually through water jet. The production parts are primarily of core/laminate sandwich construction, hence flaw resolution is generally limited by the core cell size to one-half inch. The rate of scanning depends on the equipment and the number of transducers used simultaneously.

With care, TTU can detect internal porosity in laminates down to levels where the influence on structural performance is negligible. A difficulty in using ultrasonics to inspect for porosity is differentiating porosity from other types of flaws such as matrix cracking and crazing. These problems can be solved by developing inspection standards of various material systems, thicknesses, etc., containing various levels of porosity and other flaws. Porosity detection demands dense scanning, and may require 15 min/ft² to perform.

The primary difficulties with TTU involve sandwich core. Misaligned core can disrupt the direction of the ultrasonic signals and falsely represent the damage state. Truss core construction may be difficult or impossible to scan effectively. While Kevlar is more attenuative to ultrasound than graphite composites, hybrids of graphite and Kevlar have presented no particular scanning problems. Sections of structure unreachable by automated TTU methods such as stiffeners are usually scanned with hand held TTU devices or with pulse echo.

X-Ray Radiography—X-ray methods are occasionally used to inspect for porosity and cracking in laminates, and for core anomalies in sandwich panels. Radiography is generally a procedure too slow for use in production quality control, and is difficult for field inspections. However, radiography may be used to more carefully inspect defects found with ultrasonic NDE methods.

Pulse Echo—Pulse echo is currently the favored method for field NDE because the equipment is portable. Generally, the inspector uses a single transducer to obtain a signal amplitude on an oscilloscope and marks defect locations on the surface of the panel or structure.

Boeing has constructed an experimental multiple array pulse echo transducer with its associated monitoring electronics using principles taken from a similarly operating medical device. Specifically, the transducer consists of 32 closely spaced elements (as shown in Figure 5), each 0.050-in wide, for a total width of 1.6 in. The design frequency of this prototype is 5 MHz, optimum for laminates up to 0.3-in thick with a practical limit of 0.5-in thick. Thicker laminates (1-in or more) could be scanned with a transducer designed to operate at lower frequencies.

This system is useful for creating images of disbonds, delaminations, impact damage and porosity. Figure 5 shows an oscilloscope view of a panel cross-section containing a flaw under the stiffener and a view of the sectioned area revealing the small delamination. These diagrams were taken from an original micrograph and photograph of the oscilloscope screen.

The output appearing on the oscilloscope creates a good image of the laminate structure, surfaces, and internal flaws. There are several proposed methods for recording and displaying the images. The scope output can be recorded on video tape for future study. Pseudo three-dimensional images may be constructed by overlapping oscilloscope images in an isometric view. Output from several transducers could be merged on a single television monitor image or collected on a data acquisition system. Very little development work has been done on this system so far, yet it already appears to be a method with practical potential.

Advanced Ultrasonic and Acoustic Emission Methods—Some advanced ultrasonic and acoustic emission (AE) techniques have been capable in the laboratory of comparing different composite material damage states, porosity, cure states, and measuring mechanical properties such as modulus and Poisson's ratio (refs. 3 and 4). So far, these methods have been limited to use on simple structures.

One method uses two ultrasonic transducers, one transmitting and one receiving, on the same side of the laminate (Figure 6). The system measures a stress wave factor or the number of reflected acoustic wave peaks received from a specified transmitted wave form. The stress wave factor depends on the input signal characteristics, transducer characteristics, system gain, reset time, threshold voltage, repetition rate, distance between transducers, etc.; therefore, results are generally comparable only when these factors are consistent. Experimenters have obtained good correlation between the stress wave factor and the number of impact events, and between the stress wave factor and tensile strength of graphite/epoxy coupons.

A variation on the above technique substitutes an AE transducer for the receiving transducer. This method also uses a stress wave factor as an indication of material condition. A system using roller transducers at a set distance apart could rapidly scan a structure. Acoustic Emission Technology Corporation has demonstrated such a system. Alternative fluid coupled transducers would provide higher quality results, but would decrease speed and ease of operation. The rapid scan method may be useful in discovering "suspect" areas of a structure which can be noted and further analyzed with more precise methods.

Another technique involves exciting an AE response from a structure using a thermal shock (Figure 7). This method has been informally tested on small panels before and after impact damage. Experimenters propose that a system could be devised for rapid scanning of large structures incorporating two roller transducers in a fixture with an attached heat lamp for the thermal shock input. A two transducer system could geometrically locate damaged or anomalous areas. A computerized AE data system could aid in developing the thermal AE technique as well as the more traditional AE methods.

STRUCTURAL DESIGN CRITERIA FOR IMPACT DAMAGE CONTAINMENT

The strength of composite structural members is affected by damage to the member. To fully exploit the weight savings potential of composite materials in strength designed structure, damage tolerance aspects of materials and design must be addressed.

Design criteria dictates that structure be capable of carrying design ultimate load with non-visible damage and limit load with visible damage. Much of the effort in design, testing, and analysis is directed towards enhancing the damage tolerance performance of composite structures. These efforts include improvements in material system, design using damage tolerant configurations, and design to enhance damage containment. The following design criteria will reduce the effects of impact damage in composite structure.

Material System—Materials must be selected that have high allowable stresses and strains and provide good damage tolerance characteristics. Studies, which include coupon testing performed under Phase I, reveal that high strain fibers and toughened resins significantly increase compression-after-impact capabilities. Material system toughness screening tests also include open hole tension and compression, and mode I and mode II fracture toughness. Thermoset and thermoplastic (PEEK) materials were included in Phase II material screening tests.

Skin Design—Design criteria affecting skin design include variations in the skin directional fiber%ages. Panels with skins consisting primarily of 45-deg plies are damage tolerant due to the low load level in the skin. In this design, the primary load carrying member is the stiffener. Grid stitching with Kevlar yarn in the area between the stiffeners has potential to restrict impact damage and inhibit growth (fig. 8). This has been demonstrated in both Phase II coupon level and three-stringer panel testing.

A skin that does not buckle at design ultimate loads retards skin/stiffener separation and is therefore more damage tolerant than skins which are allowed to buckle.

Skin-Stiffener Interface—There are several ways to enhance damage tolerance at the skin-stiffener interface. A reduced Poisson's ratio mismatch at the skin-stiffener interface will decrease the induced transverse strain differentials. This can prevent early disbonding or delamination. Stitching along the skin-stiffener interface with Kevlar thread, as shown in Figure 8, may help retard skin-stiffener separation. Mechanical fasteners attaching the skin to the stiffener were investigated on one Phase I three-stiffener panel configuration. Test results showed a 12% improvement in residual strength after severe stiffener cap damage. The key to structural integrity of a compression loaded stiffened panel after severe damage may be the stiffener-skin interface load transfer capability.

Stiffener Design—Several improvements in stiffener design are presented in Figure 9. The interface area between the stiffener flange and skin should be maximized to reduce the tendency of the stiffeners to pull off the skins. Minimizing thickness of the skin flange allows it to conform to the induced curvature of the skin and pad-up during loading. The thickness of the skin flange edge should be tapered to reduce stress concentrations along the skin-stiffener interface. Additional 0-deg plies buried in the skin beneath the stiffeners help restrict impact delamination formation and growth.

The design of the stiffener should incorporate 45-deg plies on the exterior surfaces for impact protection. Groups of 0-deg plies, when used, should be separated with 45-deg plies to enhance load redistribution if damage occurs. In the free flanges, interleaving web and flange plies may provide additional interlaminar shear paths in the event of damage. Kevlar stitching of the stiffener free flanges (Figure 9) may also improve stiffener damage tolerance.

CONCLUSIONS

Defects such as inclusions and porosity can occur during the fabrication of composite materials. Impact damage in composites can cause delaminations which degrades compression strength more than other defects and damage types. Impacts can be caused by such things as tool drops, equipment mishandling and other foreign objects.

Two areas of stiffened wing skin panel designs that are considered especially sensitive to impact damage are the skin pad-up ramp and the stiffener cap. Reduced residual strength caused by stiffener cap impact damage was demonstrated in a compression panel with stiffeners incorporating interleaved cap plies and skin/stiffener interface stitching. This strength reduction is significant, and demonstrates the need for durable stiffener designs and the consideration of NDE of the stiffeners as a last operation before the wing box is closed.

Approaches to limiting the adverse effects of impact damage on primary structure include design for damage tolerance and detection of critical damage levels. Improved NDE methods are being developed and will improve primary structure inspection efficiency. Approaches to designing damage tolerant structure include: improving material toughness; incorporating damage arrest features; and increasing strength at interfaces and discontinuities.

REFERENCES

1. Starnes, James H., Jr.; and Williams, Jerry G.: "Failure Characteristics of Graphite-Epoxy Structural Composites Loaded in Compression." NASA TM-84552, September 1982.
2. Byers, Bruce A.: "Behavior of Damaged Graphite/Epoxy Laminates Under Compression Loading." NASA CR-159293, August 1980.
3. Vary, Alex: "Acusto-Ultrasonic Characterization of Fiber Reinforced Composites." Materials Evaluation, 40, May 1982.
4. Williams, James H., Jr., et al: "Ultrasonic Input-Output for Transmitting and Receiving Longitudinal Transducers Coupled to Same Face of Isotropic Elastic Plate." Materials Evaluation, 40, May 1982. (Also available as NASA CR-3506, 1982.)

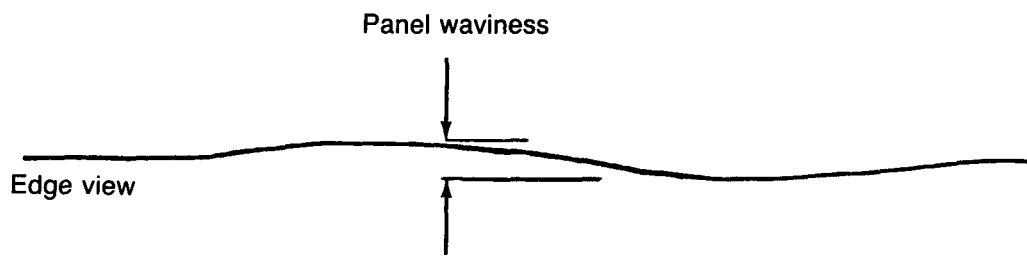


Figure 1. Contour Deviation Defect

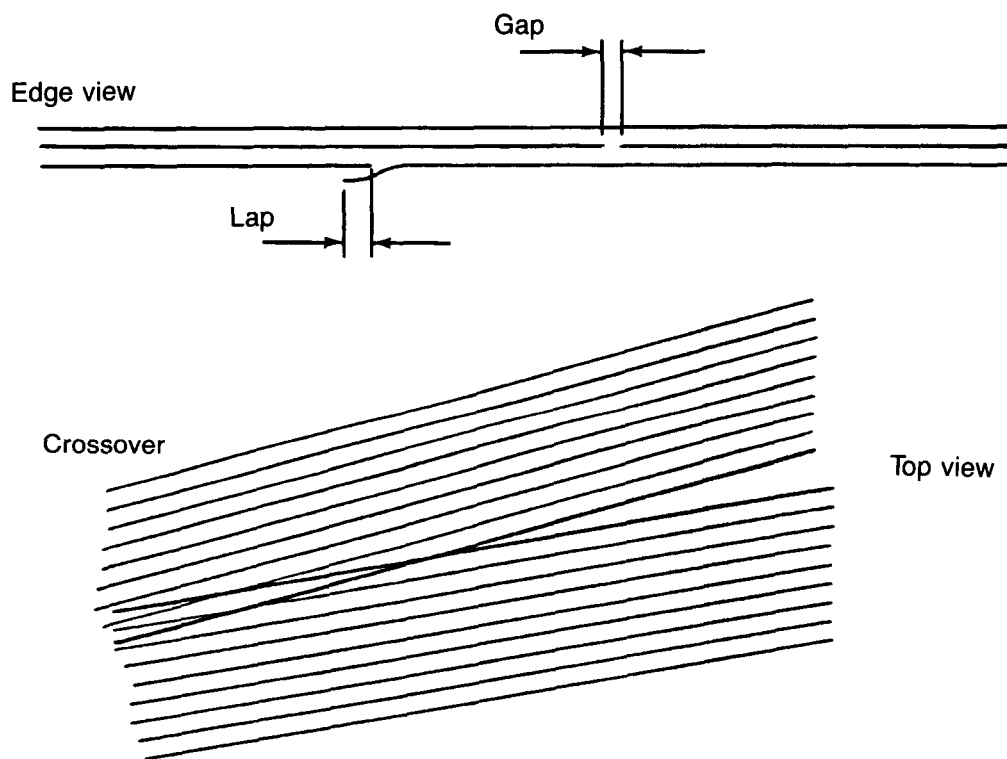


Figure 2. Ply Layup Defects

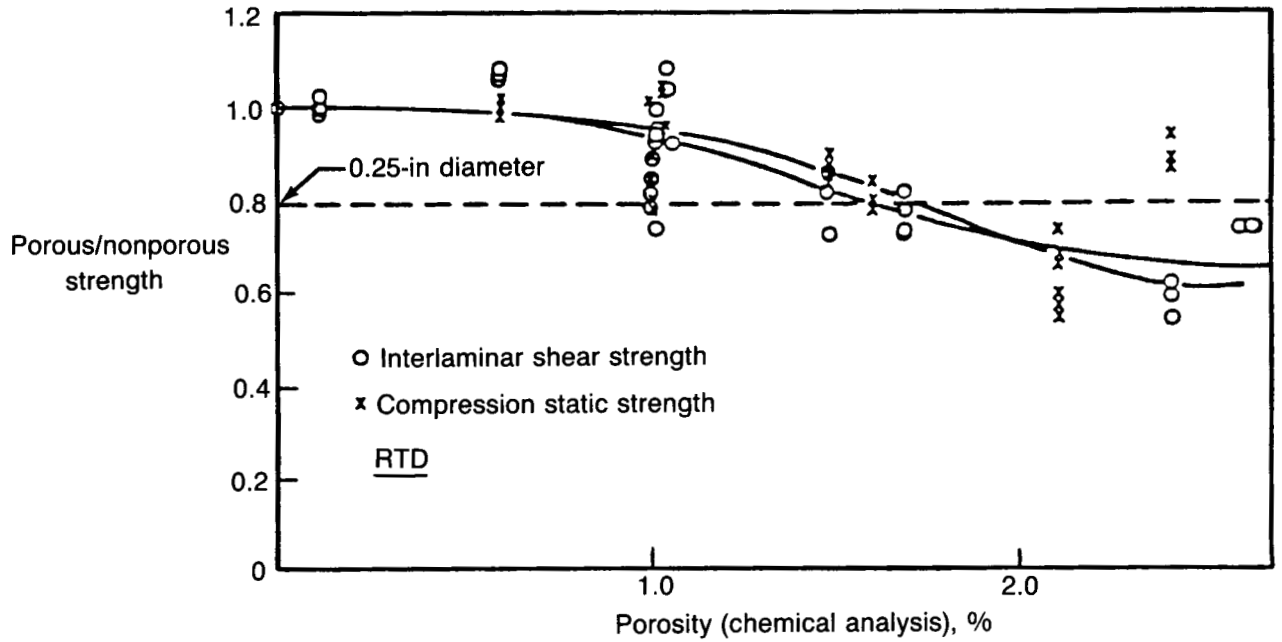


Figure 3. Influence of Porosity Level on Room Temperature Dry Interlaminar Shear and Compression Static Strength

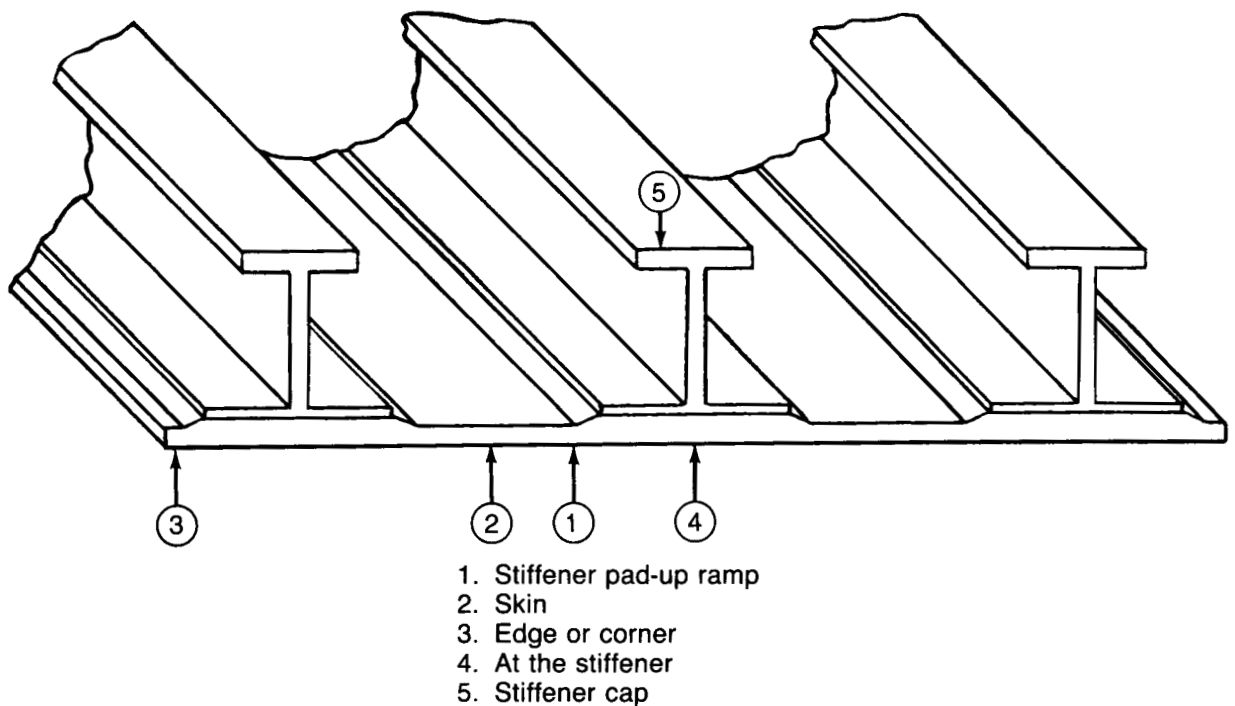
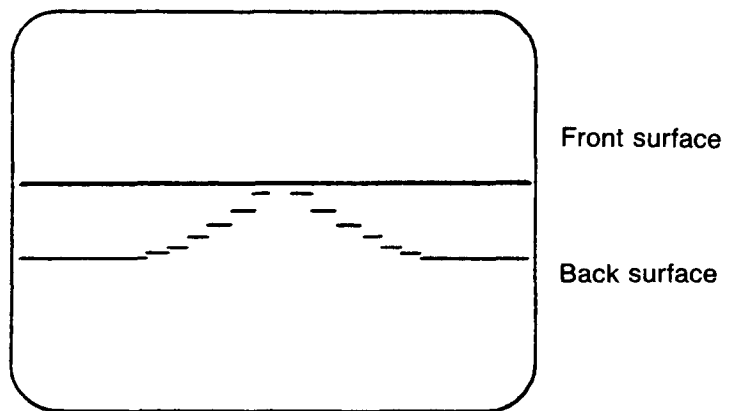
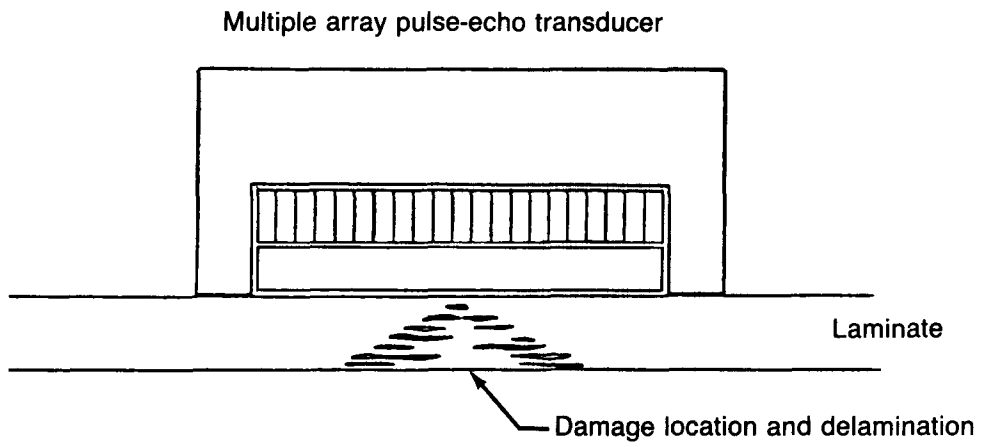


Figure 4. Critical Impact Damage Locations



Oscilloscope view

Figure 5. Multiple Array Pulse-Echo Transducer

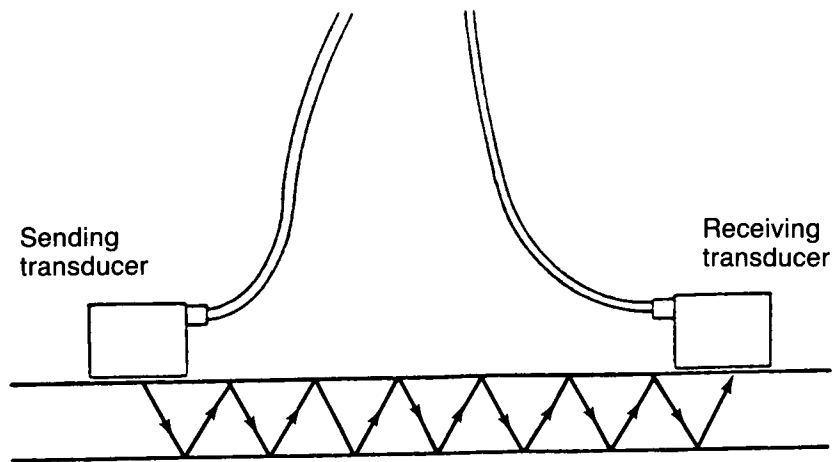


Figure 6. Two Ultrasonic Transducers

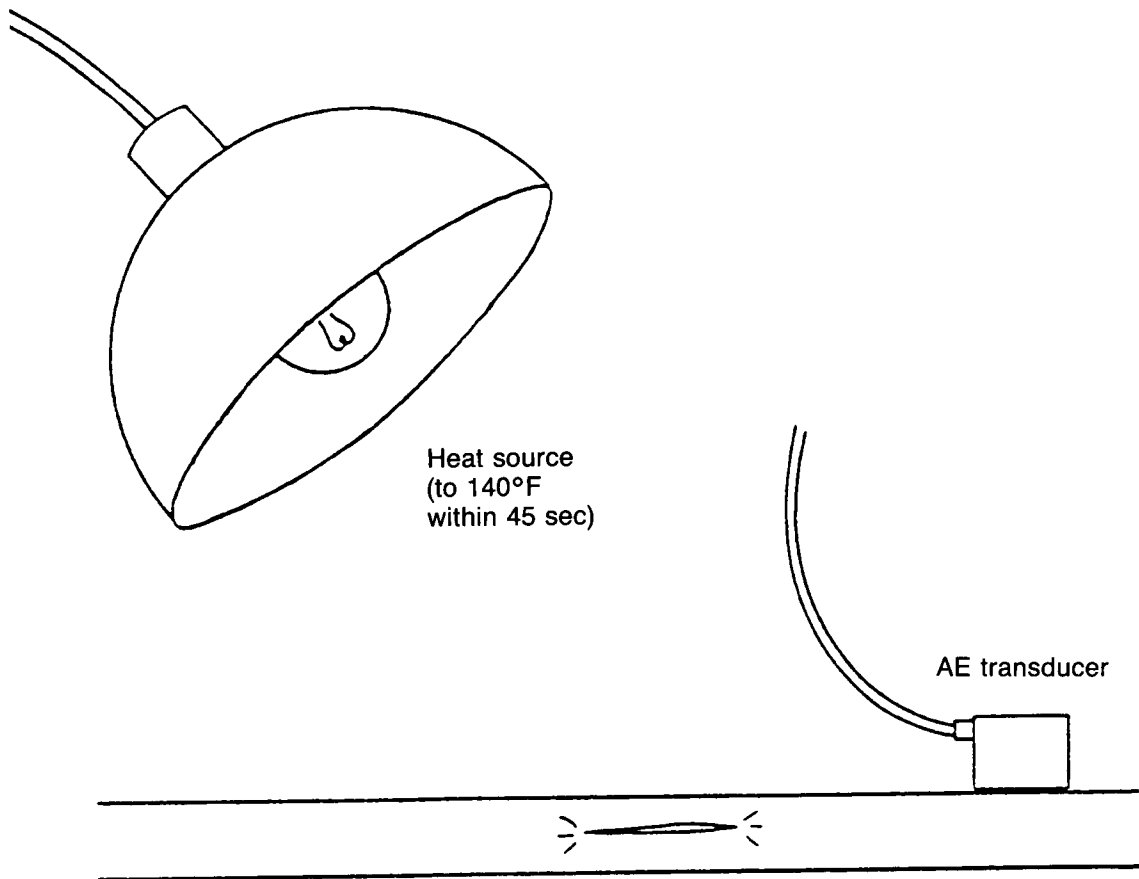


Figure 7. AE Response to Thermal Shock

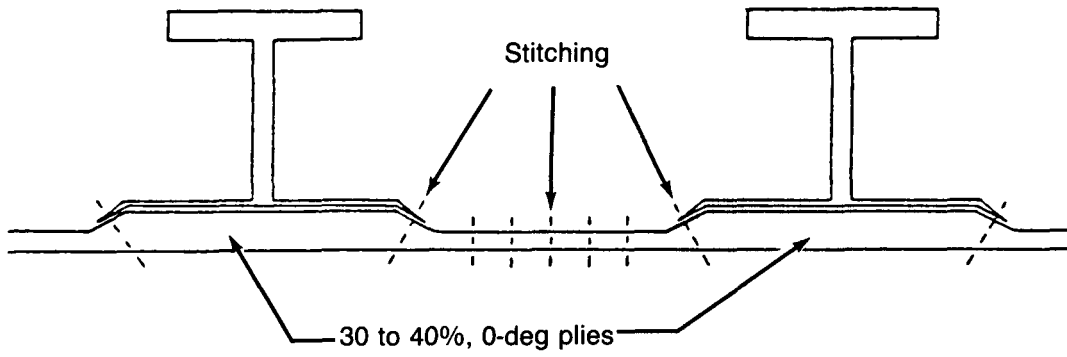


Figure 8. Structural Design Details for Impact Damage Tolerance

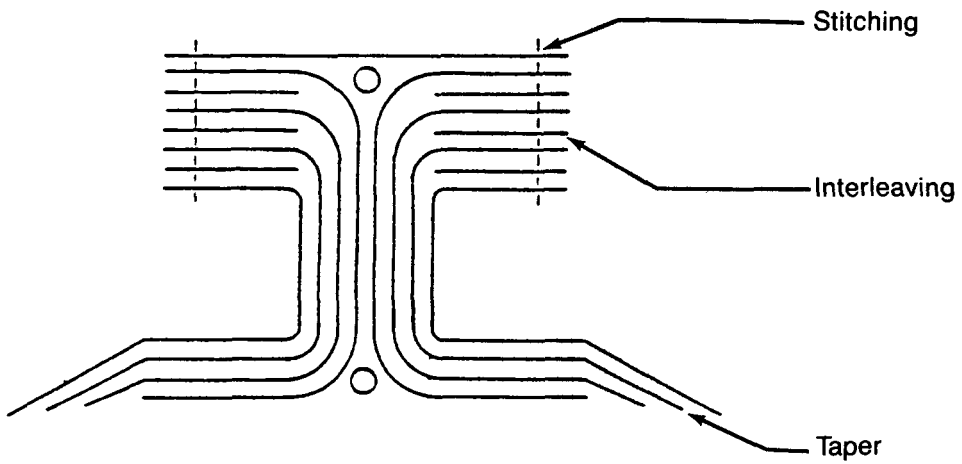


Figure 9. Structural Design Details for Impact Damage Tolerance—Stiffener

1. Report No. NASA CR-3951	2. Government Accession No.	3. Recipient's Catalog No.	
4. Title and Subtitle Damage Tolerant Composite Wing Panels for Transport Aircraft		5. Report Date December 1985	
		6. Performing Organization Code	
7. Author(s) Peter J. Smith and Robert D. Wilson		8. Performing Organization Report No.	
		10. Work Unit No.	
9. Performing Organization Name and Address Boeing Commercial Airplane Company P.O. Box 3707 Seattle, WA 98124		11. Contract or Grant No. NAS1-16863	
		13. Type of Report and Period Covered Contractor Report	
12. Sponsoring Agency Name and Address National Aeronautics & Space Administration Washington D.C. 20546		14. Sponsoring Agency Code 534-06-13-01	
		15. Supplementary Notes Appendix by M. N. Gibbins, P. J. Smith, and R. D. Wilson, Boeing Commercial Airplane Company, Seattle, Washington Langley Technical Monitor: Marvin B. Dow	
16. Abstract Analysis and testing that addressed the key technology areas of durability and damage tolerance were completed for commercial aircraft advanced composite wing surface panels. The wing of a fuel-efficient, 200-passenger airplane for 1990 delivery was sized using graphite-epoxy materials. The damage tolerance program was structured to allow a systematic progression from material evaluations to the optimized large panel verification tests. The program included coupon testing to evaluate toughened material systems, static and fatigue tests of compression coupons with varying amounts of impact damage, element tests of three-stiffener panels to evaluate upper wing panel design concepts, and a study of the wing structure damage environment. The program was completed with a series of technology demonstration tests of large compression panels. A repair investigation was included in the final large panel test.			
17. Key Words (Suggested by Authors(s)) Advanced composites Wing panels Damage tolerance Compression Commercial transport aircraft		18. Distribution Statement  Subject Category 24	
19. Security Classif.(of this report) Unclassified	20. Security Classif.(of this page) Unclassified	21. No. of Pages 60	22. Price